

## Seasonal modification of the Arctic Ocean intermediate water layer off the eastern Laptev Sea continental shelf break

Igor A. Dmitrenko,<sup>1</sup> Sergey A. Kirillov,<sup>2</sup> Vladimir V. Ivanov,<sup>3,4</sup> Rebecca A. Woodgate,<sup>5</sup> Igor V. Polyakov,<sup>3</sup> Nikolay Koldunov,<sup>6,7</sup> Louis Fortier,<sup>8</sup> Catherine Lalonde,<sup>8</sup> Lars Kaleschke,<sup>7</sup> Dorothea Bauch,<sup>1</sup> Jens A. Hölemann,<sup>9</sup> and Leonid A. Timokhov<sup>2</sup>

Received 5 December 2008; revised 28 March 2009; accepted 15 April 2009; published 11 June 2009.

[1] Through the analysis of observational mooring data collected at the northeastern Laptev Sea continental slope in 2004–2007, we document a hydrographic seasonal signal in the intermediate Atlantic Water (AW) layer, with generally higher temperature and salinity from December–January to May–July and lower values from May–July to December–January. At the mooring position, this seasonal signal dominates, contributing up to 75% of the total variance. Our data suggest that the entire AW layer down to at least 840 m is affected by seasonal cycling, although the strength of the seasonal signal in temperature and salinity reduces from 260 m ( $\pm 0.25^\circ\text{C}$  and  $\pm 0.025$  psu) to 840 m ( $\pm 0.05^\circ\text{C}$  and  $\pm 0.005$  psu). The seasonal velocity signal is substantially weaker, strongly masked by high-frequency variability, and lags the thermohaline cycle by 45–75 days. We hypothesize that our mooring record shows a time history of the along-margin propagation of the AW seasonal signal carried downstream by the AW boundary current. Our analysis suggests that the seasonal signal in the Fram Strait Branch of AW (FSBW) at 260 m is predominantly translated from Fram Strait, while the seasonality in the Barents Sea branch of AW (BSBW) domain (at 840 m) is attributed instead to the seasonal signal input from the Barents Sea. However, the characteristic signature of the BSBW seasonal dynamics observed through the entire AW layer leads us to speculate that BSBW also plays a role in seasonally modifying the properties of the FSBW.

**Citation:** Dmitrenko, I. A., et al. (2009), Seasonal modification of the Arctic Ocean intermediate water layer off the eastern Laptev Sea continental shelf break, *J. Geophys. Res.*, 114, C06010, doi:10.1029/2008JC005229.

### 1. Introduction

[2] The intermediate waters of the Arctic Ocean's Eurasian continental margins are influenced by the confluence of the warm and saline Atlantic Water (AW) inflow through Fram Strait with the denser, colder and slightly fresher AW inflow through the Barents Sea that enters the Arctic Ocean between Franz Josef Land and Severnaya Zemlya [Rudels et al., 1994; Figure 1]. The difference in characteristics between the Fram

Strait branch of AW (FSBW) and the Barents Sea branch of AW (BSBW) is mainly explained by 2 processes: (1) cooling and ventilation of the BSBW by air-sea interactions over the Barents Sea shelf [Schauer et al., 2002a, 2002b; Falkner et al., 2005] and (2) freshening due to interaction with the fresher Norwegian Coastal Current [Schauer et al., 2002a, 2002b]. The merged AW branches are found at intermediate (150–1000 m) depths and follow the Eurasian Basin bathymetry in a cyclonic sense as a narrow, topographically trapped boundary current [Timofeev, 1957; Aagaard, 1989; Woodgate et al., 2001; McLaughlin et al., 2002; Schauer et al., 2002b; Karcher et al., 2003; Polyakov et al., 2005; Dmitrenko et al., 2008a].

[3] Although rarely reported, there is actually every reason to expect seasonality in the AW boundary current. The varying inflow of the warmer and saltier AW into the Arctic Ocean is believed to correlate with the variability of large-scale atmospheric patterns [Dickson et al., 2000]. It seems that stronger cyclonic atmospheric circulation over the North Atlantic during winter drives substantial seasonality in the AW inflow into the Arctic: Ekman transport driven by winter southwesterly winds results in higher inflow of both FSBW through Fram Strait [Morison, 1991; Fahrback et al., 2001; Schauer et al., 2004] and BSBW through the Barents Sea Western Opening (BSO,

<sup>1</sup>Department of Paleooceanography, Leibniz Institute of Marine Sciences, University of Kiel, Kiel, Germany.

<sup>2</sup>Department of Oceanology, Arctic and Antarctic Research Institute, St. Petersburg, Russia.

<sup>3</sup>International Arctic Research Center, University of Alaska, Fairbanks, Alaska, USA.

<sup>4</sup>Now at Dunstaffnage Marine Laboratory, Scottish Association for Marine Science, Oban, UK.

<sup>5</sup>Polar Science Center, Applied Physics Laboratory, University of Washington, Seattle, Washington, USA.

<sup>6</sup>International Max Planck Research School on Earth System Modeling, Hamburg, Germany.

<sup>7</sup>Institute of Marine Sciences, University of Hamburg, Hamburg, Germany.

<sup>8</sup>Department of Biology, Laval University, Quebec City, Quebec, Canada.

<sup>9</sup>Alfred Wegener Institute for Polar and Marine Research, Bremerhaven, Germany.

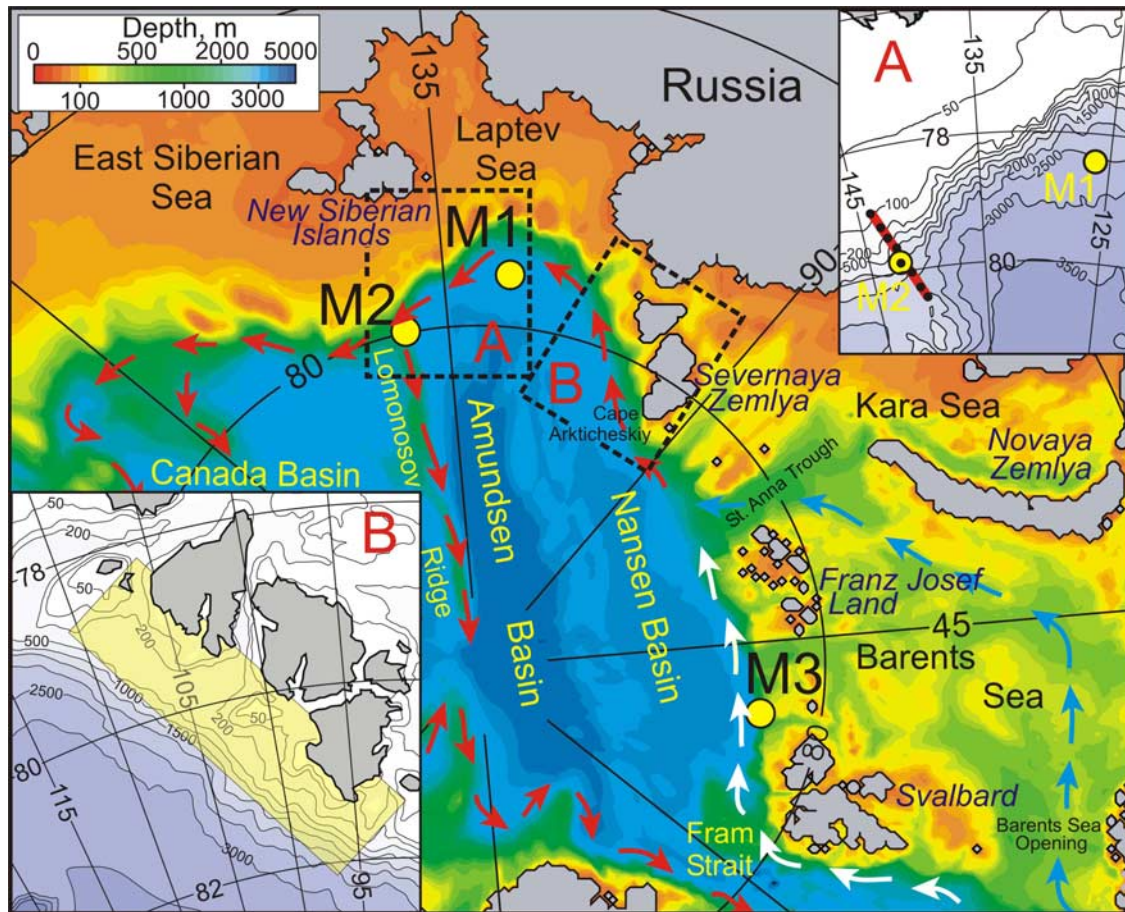


**Figure 1.** A map of the Arctic Ocean with insets showing (a) an enlarged view of the northeastern Laptev Sea region and (b) the Laptev Sea continental slope adjoining the Severnaya Zemlya Archipelago. Arrows trace the AW pathways; white and blue arrows show the Fram Strait and Barents Sea branches, respectively, of the AW inflow into the Arctic Ocean as per Rudels *et al.* [1994]. Yellow circles mark the mooring positions. Red line in Figure 1a shows CTD cross-slope transect carried out in 2003–2007. Yellow shading in Figure 1b shows location of the East Severnaya Zemlya (ESZ) coastal polynya as per Bareiss and Gørgen [2005]. Bathymetry is adapted from the International Bathymetric Chart of the Arctic Ocean (IBCAO), 2001 version [Jakobsson and IBCAO Editorial Board Members, 2001].

Figure 1) [Loeng *et al.*, 1997; Ingvaldsen, 2005; Ingvaldsen *et al.*, 2004a, 2004b]. From long-term mooring observations across the West Spitsbergen Current, for the 1997–1999 period, Fahrbach *et al.* [2001] reported a maximum FSBW monthly transport in winter (February) of 20 Sv, and a minimum of 5 Sv in summer (August). In contrast to Fram Strait, 2004–2006 mooring observations downstream on the continental slope off Spitsbergen surprisingly revealed no substantial seasonal signal in the velocity of the FSBW along-slope boundary current; with this current remaining fairly constant throughout the year [Ivanov *et al.*, 2009]. In an analysis of 1-year mooring observations in the BSO in 1997–1998, Ingvaldsen *et al.* [2002] also detected no substantial seasonal signal in the BSBW inflow transport, even though their measurements indicated current intensification, strong lateral velocity gradients, and a distinct, surface-intensified, relatively high-velocity core inflow driven by the frequent passing of atmospheric lows in the winter. During the summer the inflow area was wider than in winter, and there were two lower-velocity inflow cores. From a longer mooring record however, 1997–2001,

Ingvaldsen *et al.* [2004b] did find wind-forced intensification of the BSBW winter transport, which was typically 0.4 Sv greater than the mean summer transport of 1.3 Sv. Current measurements carried out during 1991–1992 in an array in the northeastern Barents Sea between Novaya Zemlya and Franz Josef Land ~1200 km downstream of the BSO exhibited a clear seasonal signal; with maximum flow occurring in November–February, with a peak value of 3.1 Sv in December. This value was twice as high as the minimum flow observed during the summer [Loeng *et al.*, 1993; Loeng *et al.*, 1997; Schauer *et al.*, 2002a].

[4] The seasonal temperature signal in the AW inflow is also well documented. For the FSBW inflow, multiyear measurements in Fram Strait [Quadfasel *et al.*, 1991; Schauer *et al.*, 2004] confirm the existence of a strong seasonal signal in water temperature in the West Spitsbergen Current, with minimum values in January–March. During 1980–1991 the observed surface temperature seasonal amplitude ranged between 4°C and 8°C. Using mooring observations from 1997 to 2006, U. Schauer (personal communication, 2007) suggests the seasonal amplitude in

temperature varies from 1 to 2.5°C. This seasonal signal was traced ~600 km downstream over the Nansen Basin continental slope off Spitsbergen. In 2004–2006, it exhibited a clear seasonal amplitude of ~3–4°C in the 70- to 215-m water layer, with maximum and minimum values in April–June and November–December, respectively [Ivanov *et al.*, 2009]. The BSBW seasonal signal dominates the power spectrum of temperature and salinity over the BSO [Furevik, 2001; Ingvaldsen *et al.*, 2004a]. The conductivity-temperature-depth (CTD) section across the southern BSO sampled 6 times each year from 1980 to 1996 reveals a clear seasonal cycle in temperature with minimum temperature during January–February and a seasonal amplitude of ~4–6°C. This signal retains its identity over the Barents Sea shelf [Schauer *et al.*, 2002a; Smolyar and Adrov, 2003], and has also been documented ~1200 km downstream over the eastern Barents Sea [Loeng *et al.*, 1993; Loeng *et al.*, 1997; Schauer *et al.*, 2002a]. The 1991–1992 mooring record showed maximum temperature values in October–November (~0.8–0.9°C) and minimum values in January, when the BSBW seasonal signal has been substantially modified by local sea-ice processes [Schauer *et al.*, 2002a].

[5] The far-field effects of the FSBW and BSBW inflow are traceable thousands of kilometers downstream over the Nansen, Amundsen, and Canada basins [Carmack *et al.*, 1997; Woodgate *et al.*, 2001; McLaughlin *et al.*, 2002; Karcher *et al.*, 2003; Woodgate *et al.*, 2007; Dmitrenko *et al.*, 2008a, 2008b]. Therefore it is surprising that an AW seasonal signal driven by upstream seasonality has never been reported downstream of the FSBW and BSBW confluence in the northern Kara Sea. This paper addresses the issue of seasonal variability of the AW intermediate layer in the eastern Laptev Sea (Figure 1), the area located near the junction of the Siberian continental margin with the Lomonosov Ridge, approximately 1200 km downstream of the FSBW and BSBW confluence at the St. Anna Trough. Our paper uses the 3-year (2004–2007) mooring records of temperature, salinity, and currents from the FSBW and BSBW core depths at mooring site M2, as well as shipboard CTD sections taken across the continental slope at ~144°E near the mooring position during August–September 2003–2007. We demonstrate that the entire AW layer exhibits seasonal variability in temperature and salinity that is superimposed on the warming tendency that has been observed in this area since 2004 [Polyakov *et al.*, 2005; Dmitrenko *et al.*, 2008a]. More specifically, our study focuses on the seasonal modification of the entire AW layer that seems to occur upstream over the Kara Sea continental slope by interactions between the FSBW and BSBW inflows, and is then advected downstream along the Laptev Sea continental slope to the mooring position, still retaining distinctive seasonal properties in temperature, salinity, and water dynamics. We define the maximum cross-slope AW core temperature and velocity layer as an AW jet. The AW jet is not resolved by our single mooring observations. The maximum intermediate water layer temperature marks the FSBW core. The temperature and salinity intermediate minima over the depth range of 400–1100 m beneath the FSBW layer is defined as the BSBW core.

[6] The paper is structured as follows. Section 2 is a brief description of data. Section 3 addresses several specific aspects of time series composition that are important for

further data interpretation. Using 2004–2007 temperature, salinity, and velocity observational data, section 4 reveals the characteristic difference between seasons in terms of their water dynamics, thermohaline, and spectral properties. Section 5 puts our findings into the context of upstream thermohaline and water dynamics patterns to determine possible causes of the AW layer seasonal modification. Section 6 summarizes our conclusions and points out deficiencies in our analysis.

## 2. Data

[7] The data used in this study were collected from a conventional mooring named M2 deployed at 79°55'N, 142°21'E offshore from the eastern Laptev Sea continental shelf break near the junction with the Lomonosov Ridge (Figure 1) in ~1250-m water depth. With annual redeployments in August–September, this mooring collected data for three consecutive years (2004–2005, 2005–2006, and 2006–2007). Table 1 summarizes the instrumentation on this mooring from 2004–2007. Initially the M2 mooring was designed to sample the cores of the FSBW (~260 m) and the BSBW (~840 m). It was equipped with Sea-Bird Electronics, Inc. SBE-37s with CTD sensors placed at 39, 128, 253, and 297 m (2004–2005), 267 and 772 m (2005–2006), and 170, 216, and 781 m (2006–2007), and two Aanderaa Instruments Recording Current Meters (RCM-11s) with CTD and Doppler velocity sensors placed at 254 and 824 m (2004–2005), 275 and 839 m (2005–2006), and 280 and 856 m (2006–2007). The mooring also carried a Teledyne RD Instruments 300 kHz Workhorse Sentinel Acoustic Doppler Current Profiler (ADCP) measuring velocity through the depth range of 25–121 m (2004–2005), 58–154 m (2005–2006), and 176–256 m (2006–2007).

[8] The CTD and current meters provided 60-minute interval (RCM-11s) and 15-minute interval (SBE-37s) 3-yearlong records of velocity, conductivity, temperature, and pressure at fixed depths. The 3 years of velocity data from the ADCPs was taken at 4 m depth intervals, with a 60-minute ensemble time interval and 60 pings per ensemble. The SBE-37s at 253 m (2004–2005), 267 m (2005–2006), and 216 m (2006–2007), and RCM-11s at 254 m (2004–2005) and 275 m (2005–2006 and 2006–2007) were located near the FSBW core and measured positive temperatures throughout the year. The SBE-37s at 772 m (2005–2006) and 781 m (2006–2007), and RCM-11s at 824 m (2004–2005), 839 m (2005–2006), and 856 m (2006–2007) were located near the BSBW core and measured temperatures nearer to 0°C.

[9] Records from instruments located outside the FSBW and BSBW cores are used in this paper only to check the reliability of TS at the instruments in the cores. For example, from this comparison, the conductivity records from the RCM-11s were considered unreliable since they yielded an unrealistic salinity range of 24 to 36 psu and these records were omitted. From the ADCP data, only the ADCP record from 2006–2007 was employed in this analysis. It was used to verify the upper-level RCM-11 velocity record.

[10] Mooring-based observations were complemented by annual oceanographic CTD transects across the eastern Laptev Sea continental slope (Figures 1a and 2) taken from

**Table 1.** Summary of M2 Mooring Equipment

Period of Deployment	RCM-11 Depths (m)	SBE-37 Depths (m)	ADCP Profiling Range (m)
18 September 2004–17 September 2005	254, 824	39, 128, 253, 297	25–121
18 September 2005–27 August 2006	275, 839	267, 772	58–154
29 August 2006–21 September 2007	280, 856	170, 216, 781	176–256

the icebreaker *Kapitan Dranitsyn* (2004–2006) and the RV *Viktor Buynitsky* (2007) in August–September using a shipboard SBE19+ CTD. The maximum depth of these casts was 1100 m, and within this range, most of CTD casts were taken down to ~15–20 m above the seafloor.

[11] According to manufacturers' estimates, individual temperature and conductivity measurements are accurate to  $\pm 0.005^\circ\text{C}$  and  $\pm 0.0005\text{ S/m}$ , respectively, for the SBE-19+, and to  $\pm 0.002^\circ\text{C}$  and  $\pm 0.0003\text{ S/m}$ , respectively, for the SBE-37. RCM-11 Doppler Current Sensor precision and resolution are reported to be  $\pm 1\%$  of reading and  $\pm 0.3\text{ cm/s}$ , respectively. Compass accuracy is  $\pm 5\text{ deg}$ . The RCM-11 temperature sensor is accurate to  $\pm 0.05^\circ\text{C}$ . RDI ADCP precision and resolution are  $\pm 0.5\%$  and  $\pm 0.1\text{ cm/s}$ , respectively. The ADCP velocity estimated error was of  $0.5\text{ cm/s}$ . Compass accuracy is similar to that of the RCM-11.

[12] Monthly mean surface air temperature (SAT) over the western Laptev Sea was derived from the National Center for Environmental Prediction/National Center for Atmospheric Research (NCEP/NCAR) reanalysis data set. The horizontal resolution of the NCEP-derived data is  $2.5^\circ$  of latitude and longitude. Sea-ice concentration data are from the AMSR-E ASI ice concentration data set which has a grid cell size of  $6.25 \times 6.25\text{ km}$  [Spren and Kaleschke, 2008]. Sea-ice concentrations were calculated with the ARTIST (Arctic Radiation and Turbulence Interaction Study) sea-ice (ASI) concentration algorithm using AMSR-E 89 GHz brightness temperatures [Spren et al., 2008]. The sea-ice daily mean and SAT monthly mean data were collected and averaged for 2003–2007 over the area of the East Severnaya Zemlia (ESZ) coastal polynya shown in Figure 1b according to Bareiss and G6rger [2005]. The sea-ice extent (SIE) over the

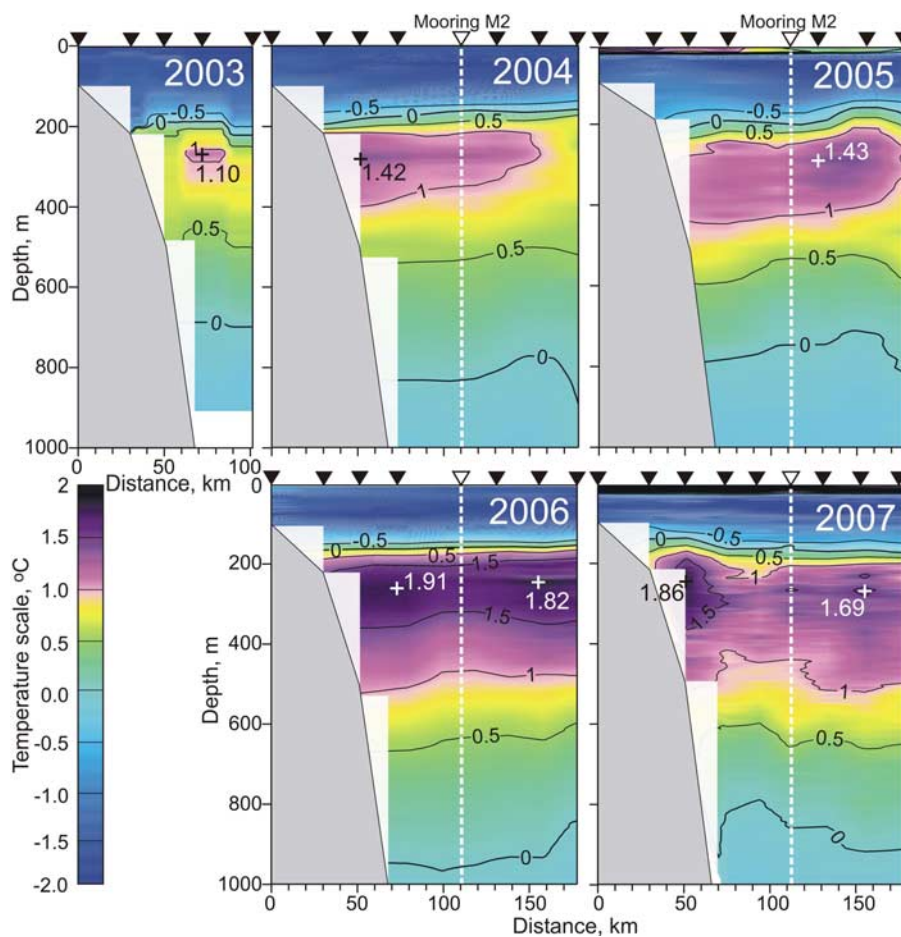


**Figure 2.** The 10-m binned temperature ( $^\circ\text{C}$ ) cross-slope sections taken in August–September 2003–2007 across the eastern Laptev Sea continental slope (see Figure 1a). The vertical white dashed line shows the M2 mooring position. Black arrows on the top of each panel show the CTD stations. The northern end of the 2003 section lies at the mooring position in 2004–2007. The numbered black and white crosses show the FSBW jet core location and temperature.

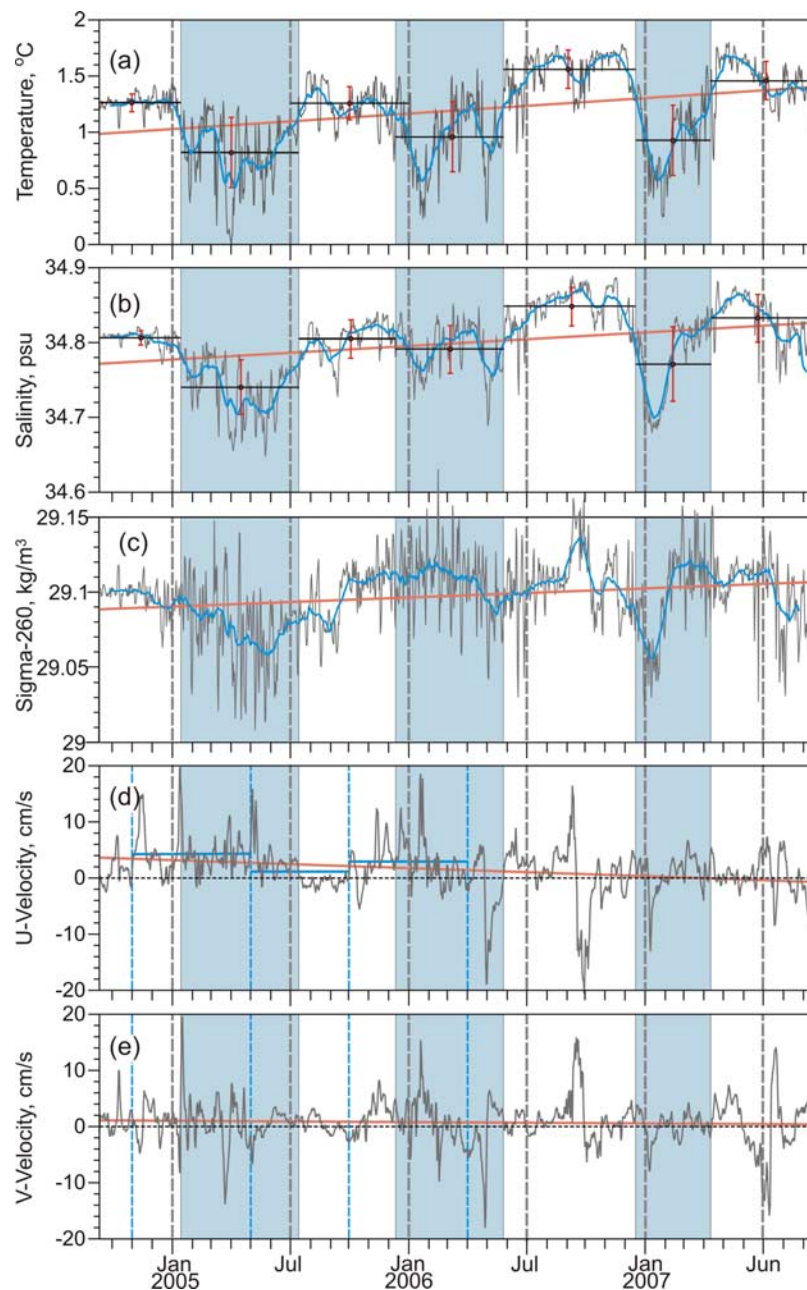


**Figure 3.** The 3-yearlong daily mean time series of (a) temperature ( $^{\circ}\text{C}$ ), (b) salinity (psu), (c) sigma-260 ( $\text{kg}/\text{m}^3$ ), (d) zonal and (e) meridional current velocity ( $\text{cm}/\text{s}$ ) from the FSBW core ( $\sim 260$  m) at the M2 mooring. The 30-day running mean (blue line) of temperature and salinity exhibits seasonal variability, with warmer and saltier water during the “high” season and cooler and fresher water during the “low” season, as emphasized by blue shading. The “high” and “low” velocity seasons delineated by blue dashed lines do not coincide with thermohaline seasonality. The seasonal mean is depicted by horizontal lines. Error bars show  $\pm 1$  standard deviation of the seasonal mean. The linear trends are shown by bold red lines.

ESZ polynya area was defined as the area of all  $6.25 \times 6.25$  km grid cells with ice concentration higher than 15%.

### 3. Data Quality and Processing

[13] The data quality is generally good with the exception of salinity data from the RCM-11s which were omitted from this analysis. In contrast to the salinity data, high correlations between SBE-37 and RCM-11 temperature records

from adjacent depth levels (not shown) supports the quality of the RCM-11 temperature data. The RCM-11 velocity record quality is confirmed by high correlations with the ADCP-derived velocity data from the adjacent level within the FSBW layer (2006–2007 only, not shown). Although the SBE-37s and RCM-11s were not calibrated between 2004 and 2007, no substantial trend in temperature and salinity is found in the data, and the majority of mooring-

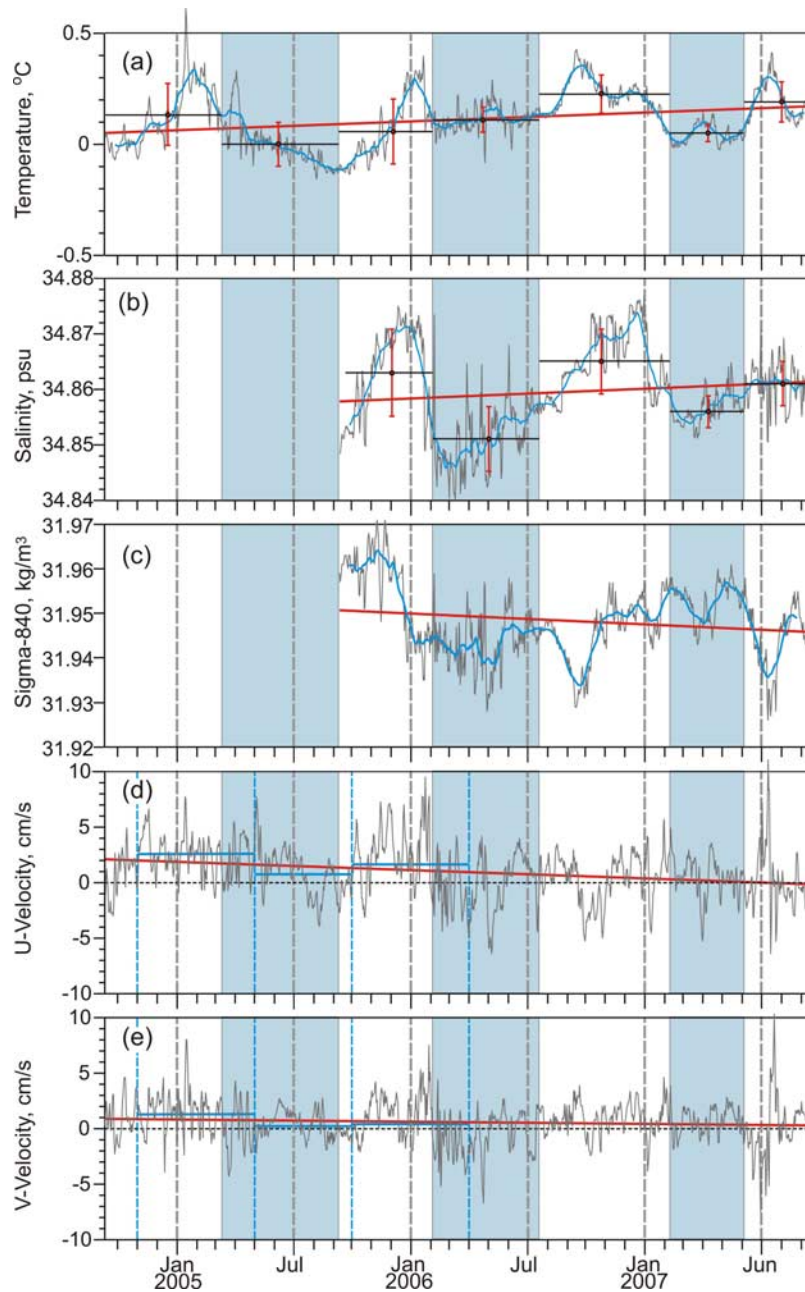


**Figure 4.** The 3-yearlong daily mean time series of (a) temperature ( $^{\circ}\text{C}$ ), (b) salinity (psu), (c) sigma-840 ( $\text{kg}/\text{m}^3$ ), (d) zonal and (e) meridional current velocity ( $\text{cm}/\text{s}$ ) from the BSBW core ( $\sim 840$  m) at the M2 mooring. The 2004–2005 salinity and density records are missing. As of the 260 m, the 30-day running mean (blue line) of temperature and salinity exhibits seasonal variability. Note that temperature and salinity seasons shown by shading are lagged relative to the FSBW core seasons by  $\sim 50$  days. The “high” and “low” velocity seasons delineated by blue dashed lines do not coincide with thermohaline seasonality. The seasonal mean is depicted by horizontal lines. Error bars show  $\pm 1$  standard deviation of the seasonal mean. The linear trends are shown by bold red lines.

based records agree well (to within errors) with CTD casts taken annually at the mooring position during mooring turnaround. The shipboard CTD was calibrated by the manufacturer (Sea-Bird Electronics, Inc.) before each cruise. The composite 2004–2007 time series of temperature and salinity for the FSBW core ( $\sim 260$  m, Figures 3a and 3b) and the BSBW core ( $\sim 840$  m, Figures 4a and 4b) were drawn from SBE-37 and RCM-11 mooring records

and CTD profiles taken at the mooring position during deployment/recovery cruises of 2004–2007.

[14] The following procedure was employed for data processing. First, all SBE-37 pressure readings were checked to verify that they fell inside the interval of  $\pm 5$  m from the mean depth level of the instrument. The RCM-11 pressure sensor data were not used because of very poor accuracy and resolution. On average, about 2% of readings

were excluded from further analysis, when devices were carried far below the assigned depths of deployment, probably as a result of substantially increased current speed. Gaps in the data which appeared after this procedure were filled in by linear interpolation.

[15] In a second step, all time series data were averaged over a 1-day interval to remove noise and high-frequency tidal and inertial oscillations. The data gaps between mooring recovery and redeployment (1–2 days) were filled in by linear interpolation. The current direction was corrected by adding mean magnetic deviation (–10.15 deg), calculated for the mid-time of 3-year deployment [2006] with the International Geomagnetic Reference Field Model 10 (IGRFM10) (<http://www.ngdc.noaa.gov/IAGA/vmod>).

[16] Finally, the SBE-37 temperature and salinity records from the FSBW layer at 253 m (2004–2005), 267 m (2005–2006), and 216 m (2006–2007) were adjusted to the target depth of 260 m by correcting each daily mean value by

$$\delta_i = \Delta z \left( \frac{\partial \psi}{\partial z} \right)_{depl} + \left[ \left( \frac{\partial \psi}{\partial z} \right)_{rec} - \left( \frac{\partial \psi}{\partial z} \right)_{depl} \right] \frac{i \Delta z}{N},$$

where  $\psi$  indicates tracer of temperature or salinity,  $\Delta z$  is the difference between the actual depth of measurements and a target depth (260 m), and  $\partial \psi / \partial z$  is the vertical gradient of  $\psi$  between the actual depth of measurements and a target depth (260 m). The  $\partial \psi / \partial z$  was derived from the CTD profiles taken at consecutive mooring deployments and recoveries;  $N$  is the number of days between deployment and recovery; and index  $i$  indicates the current day number starting from the date of deployment. This adjustment procedure assumes that thermohaline properties change linearly through both the depth range between the actual depth of measurements and a target depth of 260 m, and the entire observational period between mooring deployment and recovery.

[17] The same procedure was applied to adjust the SBE-37 salinity records from 772 m (2005–2006) and 781 m (2006–2007) to the target depth of 840 m (~BSBW core). The temperature time series for this level, however, were calculated from the RCM-11 temperature records from the depths of 824 m (2004–2005), 839 m (2005–2006), and 856 m (2006–2007) which were closer to the target depth than the SBE-37s. The velocity records from the RCM 11s were conventionally assigned to the target depths with no data adjustment.

## 4. Results

### 4.1. Background Atlantic Water Layer Oceanography

[18] Here we document the recent AW warming at the M2 mooring site through the analysis of 2003–2007 observational data from summer snapshot CTD transects crossing the slope at the M2 mooring position (Figure 1a). The CTD transects from 2003–2007 indicate that the M2 mooring site samples the AW anomaly warming seen in the region since 2004 [Polyakov *et al.*, 2005; Dmitrenko *et al.*, 2008a]. Figure 2 shows the warming tendency of the AW layer that is consistent with the warming trend exhibited by the M2 mooring temperature record (Figures 3a and 4a), which has also been previously reported by Polyakov *et al.* [2007] and Dmitrenko *et al.* [2008a]. In February–August 2004 the

upstream mooring M1 (see Figure 1 for mooring position) measured a sudden FSBW temperature increase totaling  $\sim 0.8^\circ\text{C}$  [Polyakov *et al.*, 2005; Dmitrenko *et al.*, 2008a]. This warming was attributed to the downstream propagation of a warmer FSBW anomaly that was first recorded in Fram Strait in March 1999 [Schauer *et al.*, 2004], then detected further downstream in the northern Laptev Sea in February 2004 [Polyakov *et al.*, 2005], and finally measured along the Lomonosov Ridge in August 2005 [Dmitrenko *et al.*, 2008a]. The propagation speed of this anomaly along the Amundsen Basin margin has been estimated to be  $\sim 2$  cm/s [Dmitrenko *et al.*, 2008a]. The downstream CTD cross-slope section occupied in summer 2003 and 2004 provides further evidence that between 2003 and 2004 the warmer FSBW anomaly was found across the Laptev Sea continental slope (Figure 2, top) by this time. This change (between 2003 and 2004) is the largest seen in the record that now extends to 2007 (Figure 2). Within this record, the FSBW jet is found to warm from  $\sim 1.10^\circ\text{C}$  in 2003 to  $\sim 1.91^\circ\text{C}$  in 2006. Yet, in 2007 the FSBW jet temperature was less than  $1.87^\circ\text{C}$  (Figure 2, bottom).

### 4.2. Mooring Time Series Description

[19] The temperature and salinity records from 260 m are dominated by variability which is consistent with a seasonal cycle combined with a background positive trend of  $0.14^\circ\text{C}/\text{year}$  and  $0.016$  psu/year in temperature and salinity, respectively (Figures 3a and 3b). The background positive tendency has been attributed to the downstream propagation of the AW warm anomaly first recorded in Fram Strait in 1999 [Schauer *et al.*, 2004] and which then propagated along the Amundsen and Nansen basins' margins toward the North Pole [Polyakov *et al.*, 2005; Dmitrenko *et al.*, 2008a]. Within the seasonal cycle at M2, we identify a “low” season with cooler and fresher water from December/January to May/July, and a “high” season with warmer and saltier water from May/July to December/January (Figure 3). The classification of “low” and “high” seasons is made by considering when the 30-day running mean of daily temperature from the FSBW level crosses the 3-year linear trend and is insensitive to the exact number of days used to determine the running mean within the range of 17–41 days. A striking feature of the seasonal variations is that the winter (low season) salinity is lower than summer (high season) salinity (Figure 3b). This is contrary to the seasonality one would expect from local sea-ice formation, suggesting the salinity signal observed is not driven by local surface freezing. The mean amplitude of the FSBW seasonal variability is about  $0.51^\circ\text{C}$  and  $0.06$  psu in temperature and salinity, respectively (Table 2). The temperature and salinity standard deviation during the “low” season is  $\sim 30\%$  greater than during the “high” season. It is noteworthy that the T-S ranges of the “low” and “high” seasons show almost no overlap (Figure 3 and Table 2). The M2 temperature and salinity seasonality, with low values in winter is consistent with a 1-yearlong temperature and salinity record from the same area reported by Woodgate *et al.* [2001]. They attribute an observed  $-1^\circ\text{C}$  and  $-0.1$  psu anomaly in January–April 1996 to the along-margin propagation of a signal from the Barents Sea outflow. However, as their data is only 1 yearlong that change was not considered as a seasonal effect.

**Table 2.** Seasonal Mean Thermohaline Characteristics and Their Standard Deviations for the FSBW and the BSBW<sup>a</sup>

	FSBW (~260 m) “Low” Season		FSBW (~260 m) “High” Season		BSBW (~840 m) “Low” Season		BSBW (~840 m) “High” Season	
	T (°C)	S (psu)	T (°C)	S (psu)	T (°C)	S (psu)	T (°C)	S (psu)
2004	-	-	1.26 ± 0.08	34.81 ± 0.01	-	-	0.13 ± 0.14	-
2005	0.82 ± 0.31	34.74 ± 0.04	1.26 ± 0.16	34.80 ± 0.02	0.00 ± 0.10	-	0.06 ± 0.15	34.86 ± 0.01
2006	0.97 ± 0.31	34.79 ± 0.03	1.56 ± 0.18	34.85 ± 0.03	0.11 ± 0.06	34.85 ± 0.01	0.22 ± 0.08	34.87 ± 0.01
2007	0.93 ± 0.31	34.77 ± 0.05	1.47 ± 0.19	34.83 ± 0.04	0.05 ± 0.04	34.86 ± 0.01	0.19 ± 0.09	34.86 ± 0.01
2004–2007	0.90 ± 0.32	34.77 ± 0.05	1.41 ± 0.21	34.82 ± 0.03	0.05 ± 0.09	34.85 ± 0.01	0.15 ± 0.13	34.86 ± 0.01

<sup>a</sup>The duration of seasons is as depicted in Figures 3 and 4.

[20] Data from 840 m depth in general exhibits the same temperature and salinity patterns as in the 260 m data (Figure 4). As at 260 m, the 840 m data show a gradual increase in temperature and salinity over the record, albeit smaller in magnitude, with a seasonal cycle imposed on this trend. The timing of the seasonality is, however, different to that at 260 m. The time-lagged cross-correlation  $R$  between the 260 m and 840 m temperature records (calculated using daily means of the 3-year time series) has a maximum ( $R = 0.56$ ) at a time lag of 54 days (840 m lagging 260 m), and consideration of time lags of between 1 and 500 days only find significant (at the 95% level) correlations within the range of 42–69 days (Figure 5). The time displacement between the records at 260 and 840 m can be explained by considering the variation of current speed with depth. Woodgate *et al.* [2001] described the boundary current as equivalent barotropic [Killworth, 1992] with velocity at 800 m being only 60 to 70 % of the velocity at 250 m. The 1.5 year (2003–2005) mean velocity profile derived from the upstream M1 mooring (see Figure 1 for mooring position) also shows the AW along-slope velocity at 260 m (~2.2 cm/s) to be greater than the velocity at 700 m (1.8 cm/s) [Dmitrenko *et al.*, 2008a]. This velocity difference fits well with the 54 day lag described above for a transit from the St. Anna Trough. An alternative explanation is the along-slope advection of seasonal signal that starts out vertically displaced. The M3 mooring deployed between Svalbard and Franz Josef Land has measured a temperature maximum time displacement of about 50 days between 70 and 265 m depth [Ivanov *et al.*, 2009] and the CTD sections occupied through the BSO have shown temperature maximum delayed by ~45 day from 50 to 200 m [Furevik, 2001].

[21] Following on from our time-lagged cross-correlation analysis, we identified the “low” and “high” seasons for the BSBW layer (~840 m) by introducing a 54 day time shift relative to the FSBW seasons (Figure 4). Using other time lags in the statistically significant range of 42–69 day (Figure 5) does not substantially affect the results of seasonal mean estimations given in Table 2. However, this approach works poorly for the 840 m “low” season of 2005. The data (Figure 4a) suggest the “low” season occurred about one and a half months later than would be suggested by the 54 day time shift and this results in a slightly overestimate of the 2005 “low” seasonal mean temperature shown in Table 2 (note that the salinity record for this period is missing). This discrepancy suggests that the velocity shear between 260 m and 840 m may vary interannually, a result also suggested by the comparison of the shear quantified by Woodgate *et al.* [2001] and Dmitrenko *et al.* [2008a] discussed above. In general, the temperature and

salinity records from 840 m exhibit seasonal amplitudes of 0.10°C and 0.01 psu, which are both about 5 times smaller than those at 260 m (Figures 3 and 4, and Table 2). In contrast to 260 m, the standard deviation of temperature and salinity at 840 m is similar in magnitude in “low” and “high” seasons. Curiously, the M2 density time series exhibits no clear regularity of seasonal density modification (Figures 3c and 4c). Although this is because salinity seasons are not always the same as temperature seasons, temperature and salinity contributions to density may compensate each other, which implies the seasonality is predominantly a thermodynamic, not a dynamic effect.

[22] The 3-year mean velocity record from the FSBW core shows a flow heading of 64 deg (true) almost aligned along isobaths with a mean speed of 1.6 cm/s (Figures 3d and 3e). At the depth of the BSBW, the flow is slightly weaker (1.1 cm/s), but with virtually the same heading (59 deg true, the same within errors) as is expected from a topographically steered current (Figures 4d and 4e).

[23] A very curious feature of the velocity record is over the 3 years the mean along-slope AW current weakens and turns in direction (Figures 3 and 4). The 2004–2005 and 2005–2006 records have a deployment-mean flow of FSBW eastward along the slope toward the Canada Basin at 3.0 cm/s (heading 71 deg true), and 2.1 cm/s (heading 66 deg true), respectively. In contrast, the 2006–2007 record length mean northwestward flow of 0.7 cm/s at 328 deg (true). The BSBW flow demonstrates a similar tendency to slow from 1.9 cm/s at 63 deg true in the 2004–2005 record-length mean to 1.0 cm/s at 76 deg true in 2005–2006 mean. The 2006–2007 mean exhibits further weakening (to 0.7 cm/s) accompanied by turning north (to 20 deg true) almost aligning with the western flank of the

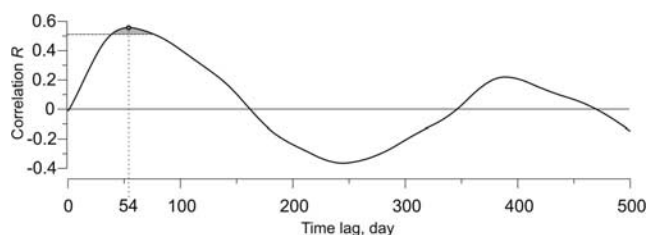


**Figure 5.** Time-lagged cross-correlation  $R$  between the M2 mooring 30-day running mean time series of temperature from 260 m and 840 m exhibits the highest correlation at a time lag of 54 days ( $R = 0.56$ ). Gray shading shows statistically significant range of correlation at 95% confidence level for the effective number of degrees of freedom  $N = 15$ .

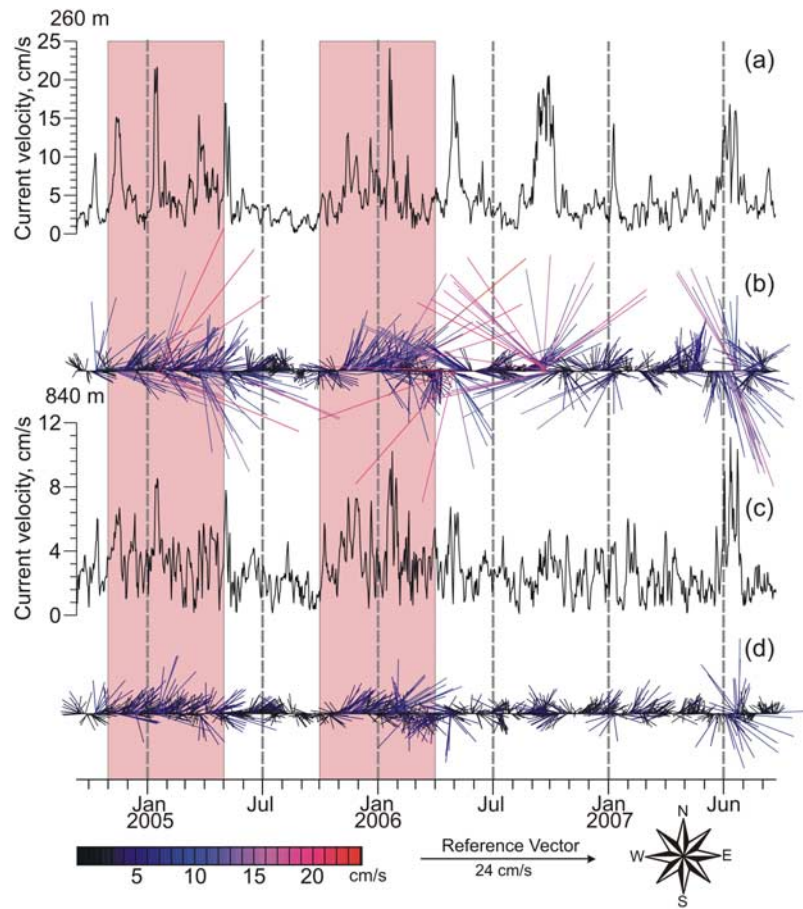


**Figure 6.** Current magnitude and stick plots of daily mean velocities from (a and b)  $\sim 260$  m and (c and d)  $\sim 840$  m. The length, color, and direction of each stick give the magnitude and direction of the 24-hour mean current. The “high” velocity seasons are shown by red shading.

Lomonosov Ridge. The velocity record (both the zonal and the meridional flow) from the FSBW layer has the best correlation (0.74, significant at 95 %) with the BSBW layer at zero time lag.

[24] Common to both the FSBW and the BSBW flow is a relatively weak seasonal velocity cycle. During 2004–2006 any seasonal cycle was strongly masked by high-frequency flow variability, and beginning in summer 2006 the seasonal cycle in velocity had disappeared or was completely masked by several isolated flow events, each lasting for more than 60 days (Figure 6). Between November and April of 2004–2005 and 2005–2006 the AW flow exhibited stronger northeastward flow (seasonal mean of 4.3 cm/s at 76 deg true and 3.1 cm/s at 71 deg true, respectively). In contrast, from May to October 2005 the FSBW flow was weaker (1.2 cm/s) and slightly turned to the east (84 deg). The BSBW flow exhibits the same patterns: between November and April it was stronger (2.8 cm/s and 1.6 cm/s at 63 deg true for 2004–2005 and 2005–2006, respectively), while between May and October 2005 the flow was weaker (0.8 cm/s) and slightly aligned toward the east (78 deg true). In fact, there is some subjectivity in determining the seasonal cycle in velocity, due to the strong high-frequency flow variability, and the comparatively low background velocity magnitude. However, it appears that any reasonable choice results in a weak seasonal cycle in velocity that lags

the temperature and salinity seasonal cycles by 45–75 days (Figures 3, 4, and 6).

[25] The strongest currents, up to 25 cm/s at both FSBW and BSBW levels, occur in isolated events lasting from several days to one month (Figure 6). Rapid turning of the currents with time is observed through our velocity record (Figures 3, 4, and 6) and likely indicates the passing of an eddy or meander [Woodgate *et al.*, 2001]. Most of these velocity features extend through the entire AW layer (Figures 3, 4, and 6); this is confirmed by a relatively high statistically significant correlation (0.74) between velocity records from 260 and 840 m. The core depth is not evident from our two-level fixed-depth observations, while the thermohaline structure exhibits both temperature and salinity negative anomalies relative to the ambient surrounding water (Figures 3 and 4). The full analysis of eddy-like features is beyond the scope of this paper. However, in the discussion which follows we will consider their temporal occurrence to address the source of seasonality observed at the M2 mooring. In subsection 4.3 we will constrain our analysis to this issue alone, by linking the seasonality of high-frequency (less than 1 cycle per month) signals in temperature and salinity with the seasonality in eddy-like, highly energetic patterns.

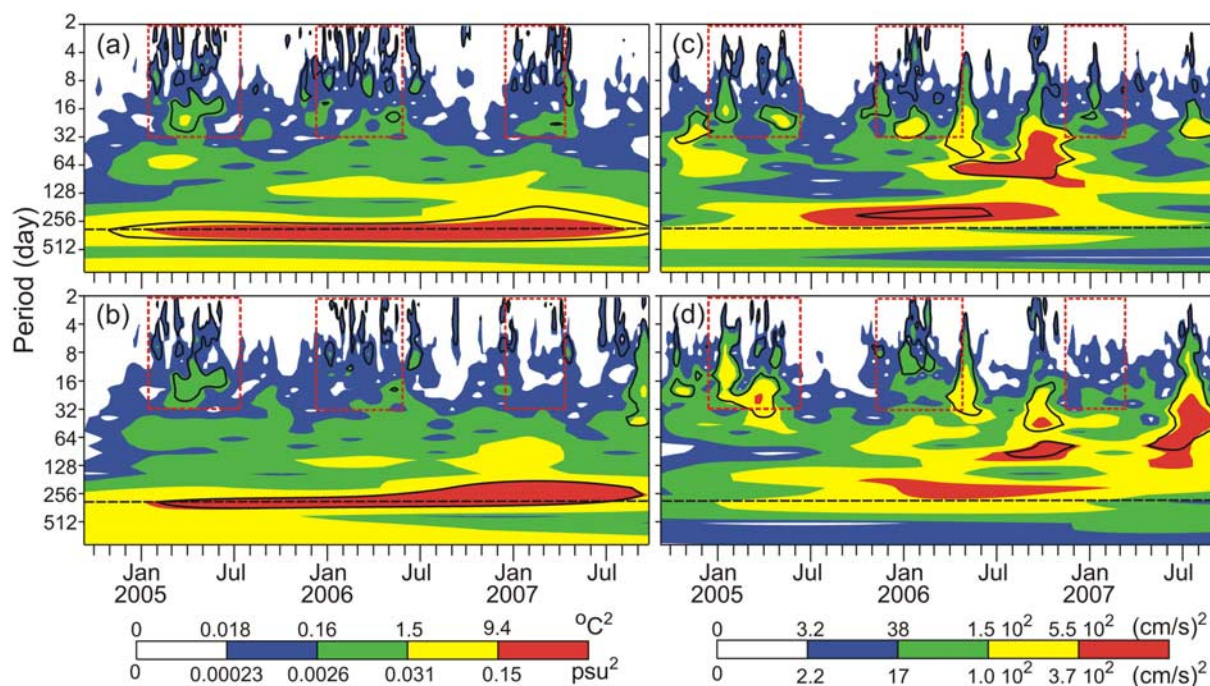


**Figure 7.** The wavelet power spectrum for the time series of (a) temperature, (b) salinity, (c)  $U$  velocity (zonal), and (d)  $V$  velocity (meridional) from  $\sim 260$  m using the Morlet wavelet transform. The contour levels are chosen so that 75%, 50%, 25%, and 5% of the wavelet power are above each level indicated by red, yellow, green, and blue, respectively, in each of the four images. The black contour lines show the 90% confidence level, using a red-noise background spectrum. The black dashed lines mark the 1-year period associated with seasonal cycling. Red dashed rectangles show the “low” seasons within a range of variability of less than 1 month.

#### 4.3. Time Series Wavelet Analysis

[26] An additional perspective on seasonality comes from a wavelet analysis. The wavelet transform method is used to analyze time series that contain nonstationary power at many different frequencies. The results of wavelet transform, presented as a contour map in the frequency/period-time plane (Figures 7, 8, and 9), allows the changing spectral composition of nonstationary signals to be measured and compared [Foufoula-Georgiou and Kumar, 1995].

[27] The wavelet power spectra for the 3-year time series of daily mean temperature and salinity (Figures 7 and 8, left) exhibits high-energy patterns (marked with dashed horizontal lines) for the time period of  $\sim 365$  days, giving qualitative evidence of seasonal modification of both FSBW and BSBW. These spectral maxima at a seasonal frequency are statistically significant at a confidence level of 90% (Figures 7 and 8, left). The wavelet power spectra shows the seasonal signal is the most energetic pattern, explaining more than 75% of the wavelet spectral energy of temperature and salinity throughout all three years of records for both FSBW and BSBW. Compared to the FSBW, the amplitude of the BSBW variability associated with seasonal cycling is reduced by  $\sim 8$  times for temperature and  $\sim 5$  times for salinity (see the color scale for Figures 7 and 8, left). Note, however, that the 3-yearlong time series are not long enough to draw reliable quantitative conclusions from the wavelet analysis in a frequency band of lower than one cycle per year.

[28] The wavelet plots also indicate that the higher spectral energy in temperature and salinity variations of less than one cycle per month was predominantly observed during the “low” seasons, contoured by red rectangles in Figures 7, 8, and 9. The energy contribution of these patterns to the entire spectrum is usually less than 25%, but most are statistically significant at the 90% confidence level. In contrast to the 2004–2005 and 2005–2006 “low” seasons, the 2006–2007 high-frequency pattern for the FSBW is less clearly defined (Figure 7, left), and none of these patterns were captured for the BSBW salinity and temperature (Figure 8, left). While the time displacement between the temperature records from 260 and 840 m has been found above, the wavelet analysis shows no time displacement in the occurrence of temperature and salinity high spectral energy patterns at 260 and 840 m (Figures 7 and 8, left).

[29] The wavelet spectrum for the velocity magnitude (Figure 9) shows seasonal cycling is not the dominant variability (compare red zones at lower frequencies). For the FSBW core (260 m), the associated narrow maximum centered at a period of 365 days is not statistically significant (see solid black contours), even though it extends throughout the entire duration of the velocity record (Figure 9a). The BSBW core exhibits a much weaker, but statistically significant seasonal maximum extending toward a lower-frequency band, but this maximum is detected only until July 2006 (Figure 9b). Perhaps this relates to the curious change in mean flow mentioned above and

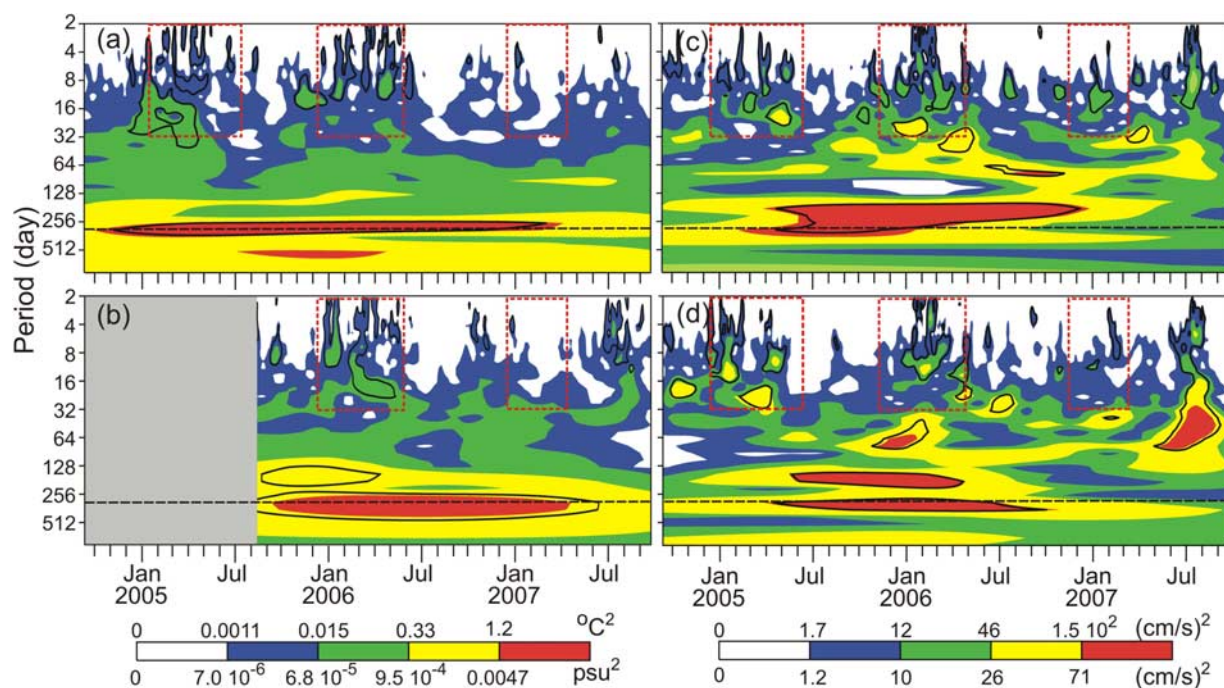


**Figure 8.** The wavelet power spectrum for the time series of (a) temperature, (b) salinity, (c)  $U$  velocity (zonal), and (d)  $V$  velocity (meridional) from  $\sim 840$  m. Gray shading in Figure 8b represents missing data. Other features including the red dashed rectangles are described in Figure 7.

expounded on below. These conclusions are echoed in the wavelet analysis of zonal and meridional velocity (Figures 7 and 8). The low-velocity value associated with the average boundary current transport (compared to the higher frequency variability) seems to be the main reason for the weaker presence of the velocity seasonal cycle in the wavelet power spectrum. Aliasing with a higher-frequency band may also corrupt the velocity seasonal maxima.

[30] The velocity wavelet spectrum for the high-frequency band demonstrates patterns similar to wavelet spectra for temperature and salinity (Figures 7 and 8, right, and Figure 9). We argue that the spectral maxima which occurred over the high-frequency band during the “low” seasons are attributable to mesoscale features (eddies and/or meanders) with a typical timescale from several days to one month. On the basis of the similarity in occurrence of high-frequency patterns in velocity, temperature, and salinity (Figures 7 and 8), we link the higher temperature and salinity variability observed during the “low” season to the eddy-like mesoscale features carried along the Siberian continental slope by the AW boundary flow (see Figure 1 for the AW circulation scheme). These patterns in the FSBW and BSBW layers seem to be linked only in the “low” seasons of 2004–2005 and 2005–2006 (Figures 7 and 8). For the “low” season of 2006–2007 the velocity record exhibits almost no energetic patterns for the high-frequency band in either the FSBW or the BSBW (Figures 7 and 8, right). We attribute this characteristic difference in high-frequency dynamics to the substantial changes which occurred in the low-frequency band. As discussed above, the 2004 to 2007 velocity data show a slowing tendency of the AW along-slope flow resulting in its gradual disappearance (Figures 3 and 4). Beginning in summer 2006, the eastward along-

slope water transport toward the Canada Basin through the junction between the continental slope and the Lomonosov Ridge switched to a much weaker flow toward the north, approximately aligned with the western flank of the

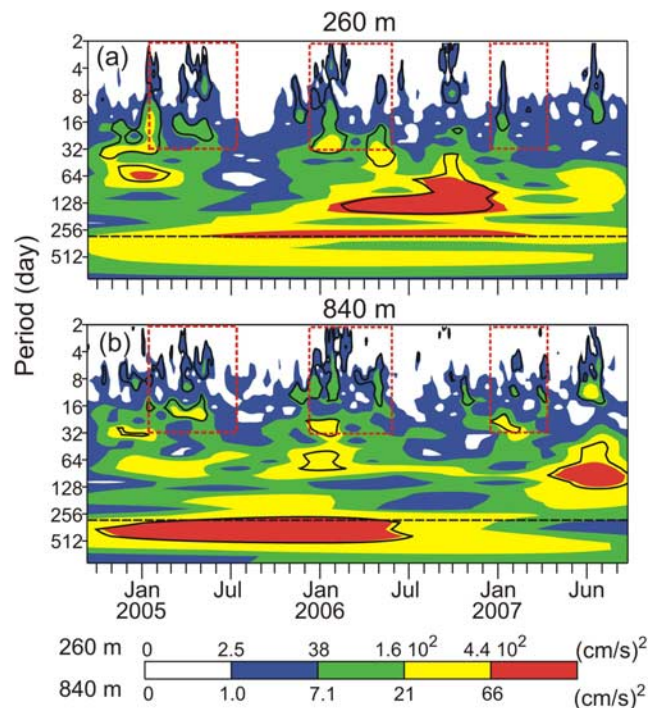


**Figure 9.** The wavelet power spectrum for the time series of velocity magnitude from (a)  $\sim 260$  m and (b)  $\sim 840$  m. Features are described in Figure 7.

Lomonosov Ridge. A weaker AW flow seems to have disrupted the seasonal pattern of the high-frequency spectra beginning in summer 2006 (Figures 7 and 8). For example, two eddy-like features from September–October 2006 and June–July 2007 substantially dominated the FSBW dynamics for almost 60 days (Figure 7). In contrast, the majority of eddies/meanders observed before September 2006 typically occurred on a timescale of 7–10 days (Figure 7). A redistribution of spectral energy to the lower-frequency band beginning in summer 2006 is also evident from the wavelet velocity spectrum (Figures 7 and 8, right).

## 5. Discussion: Potential Drivers of M2 Seasonality

[31] We argue that low/high season differences discussed above are due to the seasonal cycle. Strong seasonal variations of the thermohaline signal upstream in Fram Strait and the BSO were mentioned in the introduction. Thus it should come as no surprise that a seasonal modulation of the AW properties occurs downstream in the eastern Eurasian Basin. Indeed, our data provide evidence that the seasonal cycle exists. We consider next the mechanisms which may deliver a seasonally varying signal to the M2 site. It is possible, for example, that the observed decrease/increase in AW temperature and salinity over the Laptev Sea continental slope is governed not only by a change of the AW thermodynamic state, but also by a dynamically driven seasonal shift of the AW jet relative to the continental slope (Figure 2) as was described for the M1 mooring by *Dmitrenko et al.* [2006]. Furthermore, the East Severnaya Zemlya (ESZ) coastal polynya recurring during January–May near the western Laptev Sea continental slope off the Severnaya Zemlya Archipelago (Figure 1b) may result in seasonal cooling and ventilation of the AW layer due to intensive freezing and sea-ice formation [*Martin and Cavalieri*, 1989; *Ivanov and Golovin*, 2007; *Walsh et al.*, 2007]. Here we address the causes underlying AW layer seasonal variability by testing the characteristic signature and possible magnitude of different mechanisms including cross-slope shifting of the AW jet (section 5.1), coastal polynya ventilation (section 5.2), and advection of the seasonal signal from upstream with FSBW and/or BSBW flow (sections 5.3 and 5.4).

### 5.1. Cross-Slope Shifting of the AW Flow Jet

[32] Spatial shifting of the AW jet across the basin margins, whether driven by wind, topography, or dynamical instability, produces an observable TS change which is “noise” for our current purposes. Seasonal cycling and/or thermodynamic warming would need to rise above this level to be properly detected by a single mooring record which does not necessarily remain in the AW jet and therefore may contain variability attributed to shifting of the AW jet across the basin margins. The cross-slope CTD transects from 2003–2007 provide the background information about cross-slope migration of the FSBW jet that will be employed below for interpretation of mooring records following the approach introduced by *Dmitrenko et al.* [2006, 2008a].

[33] *Dmitrenko et al.* [2006] were the first to infer seasonal cycling over the Nansen Basin margin due to cross-slope wind-driven seasonal displacement of the AW

jet. Over the northeastern Laptev Sea winds have an offshore component from October to April, while prevailing summer winds are weaker, turning along-shore toward the east in May–September [*Dmitrenko et al.*, 2006]. At the M1 mooring (Figure 1) the on-slope shift of the warmer AW jet was observed in response to off-slope (winter) wind, while the along-slope (summer) wind results in cooling due to off-slope AW core movement. The average range of temperature anomalies related to seasonal change in wind patterns was estimated to be  $\pm 0.3^{\circ}\text{C}$  for the upper boundary of the FSBW layer (136 and 161 m) and  $\pm 0.2^{\circ}\text{C}$  at 435 m.

[34] There are several pieces of evidence supporting our speculation that cross-slope displacement of the AW jet is not capable of imposing the magnitude of seasonal cycling observed at the M2 mooring. First, while the cross-slope CTD transect was only taken during August–September (the “high” season), for the five summer seasons of 2003–2007, all but 2005 suggest that at the time of the CTD section the FSBW jet (as determined by the temperature maximum on the section) was found on-slope relative to the M2 mooring by  $\sim 30$ –60 km (Figure 2). In 2005 the AW jet was found off-slope, in this case again about 30–60 km from the mooring site. In addition, in 2006 and 2007 a second intermediate temperature maximum was observed off-slope (Figure 2, bottom) and is possibly part of the AW branch that later turns north along the western flank of the Lomonosov Ridge (see Figure 1 for the AW circulation scheme). By the arguments of *Dmitrenko et al.* [2006], the typical winter cross-slope offshore wind would cause an offshore surface current, which moves the AW jet further onshore toward the shelf. In this context, the M2 mooring is very unlikely to be sensitive to this scenario because for the five summer seasons of 2003–2007, all but 2005 suggest that at the time of the CTD section the mooring position was always seaward of the FSBW jet (Figure 2).

[35] A second piece of evidence comes from comparing temporal (seasonal) and spatial (cross-slope) temperature variability. The cross-slope FSBW temperature standard deviation was retrieved from the annual cross-slope CTD transect (Figure 2) by computing the standard deviation for the cross-slope AW core temperatures. From each year, if we assume each CTD cast is a reasonable measure of the FSBW core temperature, we can calculate a mean and standard deviation for the FSBW core temperature. These standard deviations are 0.25, 0.19, 0.1 and  $0.18^{\circ}\text{C}$  for 2004, 2005, 2006, and 2007 respectively. The FSBW temperature standard deviation derived from the 3 years of time series data at M2 (Figure 3a) is greater than this ( $0.36^{\circ}\text{C}$ ) and the mean FSBW temperature seasonal anomaly of  $\sim 0.25^{\circ}\text{C}$  (Table 2), suggesting that the “noise” in the mooring record associated with the cross-slope movement of the jet is smaller than the variability in the mooring record. The long-term mean (1894–1990) FSBW core temperature standard deviation of about  $0.18^{\circ}\text{C}$  reported for this region by *Dmitrenko et al.* [2008a] is also much less than the M2 FSBW core temperature time series standard deviation. These comparisons, however, imply that some uncertain fraction of the seasonal variance can be caused by lateral shift introducing additional uncertainty in determining the seasonal amplitude. The BSBW demonstrates the same patterns as of the FSBW. The mean BSBW temperature seasonal anomaly of  $\sim 0.05^{\circ}\text{C}$  (Table 2) is greater than the

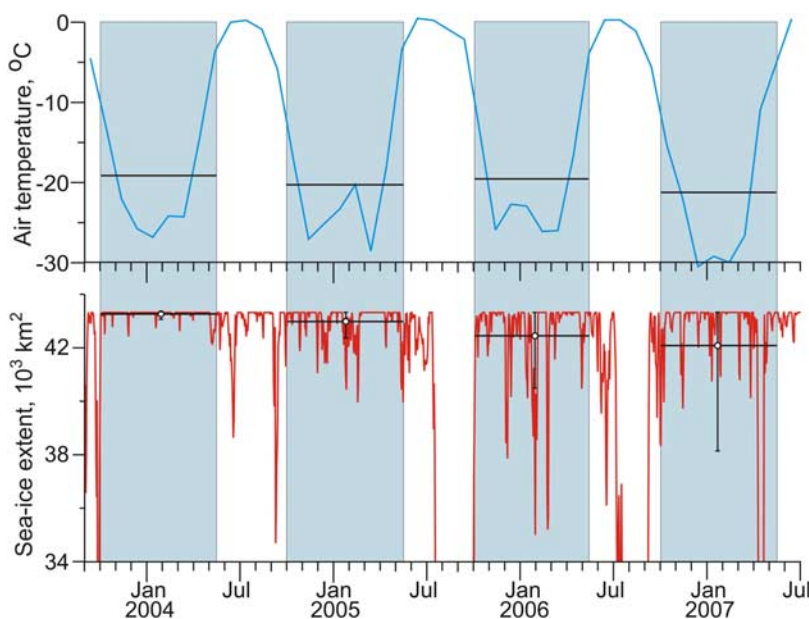


**Figure 10.** (top) Monthly mean surface air temperature (SAT) averaged over the East Severnaya Zemlya (ESZ) coastal polynya shown in Figure 1b. (bottom) The sea-ice extent (SIE) over the ESZ polynya area, defined as the area of all  $6.25 \times 6.25$  km grid cells with ice concentration higher than 15%. Minimum peaks during winter season are associated with polynya openings. Seasonal mean (1 October–15 May) SAT and SIE are depicted by horizontal lines. Error bars show  $\pm 1$  standard deviation of the winter mean SIE.

mean (2004–2007) cross-slope BSBW core temperature standard deviation of  $0.03^\circ\text{C}$ . The FSBW and BSBW core salinity demonstrates the same patterns as of the temperature.

[36] We note in passing the cross-slope FSBW temperature standard deviation is much less than the 2003–2007 warming of  $\sim 0.8^\circ\text{C}$ . This fact supports our assertion that the M2 mooring accurately captures the time variability of the AW boundary current and that this effect is larger than the effects of the AW boundary current cross-slope migration.

## 5.2. Coastal Polynya Ventilation

[37] Freezing in the coastal polynyas during winter appears to be an important influence on the transformation of AW properties during the AW boundary current transition through the western Laptev Sea [Martin and Cavalieri, 1989; Ivanov and Golovin, 2007; Walsh et al., 2007]. The system of coastal polynyas, large persistent areas of open water or young ice, on the Russian Arctic shelf, known as the Great Siberian Polynya, is believed to be a latent heat polynya [Dethleff et al., 1998], that is, the opening is driven by offshore components of the surface wind-forcing rather than by a heat source from the water. Extensive stretches of open water up to 200 km wide combined with extremely low air temperatures induce intensive ice formation, brine release, and local ventilation of the water column during winter and early spring. The coastal polynyas approximately follow the 20–25 m depth contour that over most of the Laptev Sea is about 200 km south of the continental shelf edge (Figure 1). The East Severnaya Zemlya (ESZ) coastal polynya overlying the steep continental slope off the Severnaya Zemlya Archipelago (Figure 1b) is the only exception. The shelf polynyas to the south produce water that is not dense enough to sink below the depth of the shelf edge

because the shelf waters are strongly freshened in summer by continental runoff [Schauer et al., 1997]. In contrast, the ESZ polynya located far away from riverine inputs does create waters dense enough to ventilate the AW layer, at least down to the depth of  $\sim 400$  m [Ivanov and Golovin, 2007].

[38] Our overall goals in examining the upstream ice and air temperature conditions over the ESZ polynya are (i) to estimate the variability of these conditions during the translation of the AW flow that was further recorded downstream by the M2 mooring, and (ii) to reveal their potential impact on modification of the AW properties. On the basis of the 2.4 cm/s AW boundary current velocity estimated by Dmitrenko et al. [2008a], we assume that the AW traveltime between the western Laptev Sea (where the polynya waters would enter) and eastern Laptev Sea (M2 location), a distance of  $\sim 900$  km, is about 1 year. This assumption implies a connection between the “low” seasons observed at the M2 mooring and the ESZ polynya openings which occurred one year before during January–May. We therefore examined the patterns of sea-ice extent (SIE) and surface air temperature (SAT) over the ESZ polynya in 2003–2007.

[39] The time series of monthly mean SAT averaged over the ESZ polynya region shown in Figure 1b was derived from the NCEP data set for 2003–2007 (Figure 10, top). The subsets of winter means were computed by averaging the monthly mean data from October to May, when the SAT exhibits stable values below zero. The sea-ice data were derived from the AMSR-E ASI daily sea-ice concentration data from 2003–2007 (Figure 10, bottom). The SIE is defined over the ESZ polynya region (Figure 1b) as the

area of all  $6.25 \times 6.25$  km grid cells with ice concentration greater than 15%.

[40] Through this period (2004 to 2007 winters), the SAT exhibited no substantial interannual variability (Figure 10, top). In terms of SIE, the winter mean (black circles, white filled, Figure 10, bottom) demonstrate a negative trend with almost no polynya events during winter 2003–2004, and increasing polynya presence throughout 2005–2007 (Figure 10, bottom). In contrast, the M2 temperature record demonstrates clearer seasonal modification in winter 2004–2005, while in 2005–2007 the “low” seasons were weaker. An analysis of 1984–1985 hydrographic data by *Ivanov and Golovin* [2007] revealed that under typical atmospheric forcing the dense water originating in the ESZ polynya does not penetrate deeper than 400 m. In fact, the modeled depth of density equilibrium between dense water generated by the polynya and ambient water for the 1984–1985 data was estimated to be  $\sim 200$  m [Table 1 from *Ivanov and Golovin*, 2007]. This conclusion is consistent with polynya numerical modeling by *Chapman* [1999]. A density anomaly greater than  $\sim 1$  kg/m<sup>3</sup> generated by the polynya seems unlikely for a realistic combination of atmospheric conditions, given the fact that the offshore eddy flux removes dense water from the polynya nearly as fast as ice formation can make dense water, so a quasi-steady state is achieved [*Chapman*, 1999; *Ivanov and Golovin*, 2007]. Following this conclusion, and given  $\sigma_0$  for the surface water layer over the western Laptev Sea of  $26.55$  kg/m<sup>3</sup> [*Dmitrenko et al.*, 2007] and for the BSBW layer of  $27.97$  kg/m<sup>3</sup>, one may conclude that polynya-induced vertical mixing may not affect the BSBW layer on a regular, annual basis. Contrary to this conclusion, our mooring record clearly shows that both FSBW ( $\sim 265$  m) and BSBW ( $\sim 840$  m) exhibit seasonal modification (Figures 3 and 4).

[41] The possible role of the polynyas implies an important connection between the polynya occurrence and the high-frequency AW boundary current dynamics. Primarily during the “low” seasons the M2 mooring captured eddy-like mesoscale features exhibiting cooler and fresher anomalies through the entire AW layer (Figures 3, 4, 6–9). *Woodgate et al.* [2001] suggest that these features can be generated in the Laptev Sea winter coastal polynyas from the cold and saltier water plumes produced episodically by polynya openings. Although the water in the polynya is more saline than the surrounding shelf waters, the polynya water is fresher than waters of the same density over the slope [*Woodgate et al.*, 2001]. Polynya numerical modeling by *Chapman* [2000], *Gawarkiewicz* [2000], and *Ivanov and Golovin* [2007] confirm that eddy flux plays a leading role in transporting polynya-origin water. In this context, the increase in eddy-like activity during the “low” season can be linked to a polynya. The majority of eddy-like events were traced through the entire AW layer, but it has been shown above that the ESZ polynya appears to be incapable of modifying the intermediate water layer down to  $\sim 800$  m on a regular basis. From this fact we conclude that the high-frequency AW boundary current dynamics is very unlikely to be linked to a polynya.

[42] Finally, the ESZ polynya is a temporary polynya with a frequency of occurrence of  $<50\%$  [*Bareiss and Gørgen*, 2005]. Therefore the ESZ polynya water may only occasionally become sufficiently dense to ventilate through

the entire AW layer as demonstrated for 1985 by *Walsh et al.* [2007]. It seems very likely from our mooring records that the ESZ polynya is not capable of ventilating the entire AW layer on a regular seasonal basis.

### 5.3. FSBW Inflow

[43] The seasonal signal in AW inflow through the Fram Strait (at  $79^\circ\text{N}$ ) is well documented [*Quadfasel et al.*, 1991; *Fahrbach et al.*, 2001; *Schauer et al.*, 2004]. The downstream translation of this signal with the FSBW was recently revealed by long-term observations northeast of Spitsbergen [*Ivanov et al.*, 2009]. Therefore further downstream propagation of the seasonal signal with the FSBW along the Siberian continental margin would not be unexpected. Here we compare seasonal oscillations recorded at the M2 mooring with seasonal cycling at the M3 mooring about 2200 km upstream [*Ivanov et al.*, 2009]. The M3 mooring was deployed on the Nansen Basin continental slope off Spitsbergen at a water depth of 1010 m throughout 2004–2006 (Figure 1).

[44] Turbulent heat exchange between the AW and surrounding colder water causes substantial reduction of the seasonal thermohaline amplitude (V. V. Ivanov et al., Propagation of seasonal signal in the Atlantic Water layer in the Arctic Ocean, submitted to *Journal of Physical Oceanography*, 2009). The strongest and most highly correlated seasonal oscillations of temperature (with a range of  $\sim 1^\circ\text{C}$ ) and salinity (with a range of  $\sim 0.05$  psu) at the M3 mooring were observed at 215 m (close to the FSBW core) [*Ivanov et al.*, 2009]. A similar seasonal signal with the same mean range of  $\sim 0.5^\circ\text{C}$  is well resolved in the M2 temperature record at 260 m (Figure 3a). The coincidence of salinity records from the two moorings is less obvious. Although at the M2 mooring the 12-month harmonic in the salinity record is clearly distinguishable, the shape of this harmonic is substantially distorted (Figure 3b). Besides the positive trend, which is observed in the temperature record as well, this distortion may be caused by interaction with the shelf-origin waters, discussed earlier, and with the BSBW, as demonstrated in the next subsection.

[45] Transformation of the FSBW core water properties during the transit between M3 and M2 is illustrated by the temperature-salinity (T-S) diagram in Figure 11b (note that the transit time between these sites is likely order a few years). Following the approach introduced by *Ivanov et al.* [2009], we distinguish between “high” (warmer and saltier) season and “low” (colder and fresher) season AW types for the M3 mooring using the regression line to the T-S scatter. Downstream transformation of water properties is predominantly isopycnal, that is, temperature and salinity changes compensate each other, resulting in a very tiny change of potential density. In “high” season the mean potential density of the water increases by  $0.03$  kg/m<sup>3</sup>, while in “low” season the density anomaly is negative and is less than  $0.01$  kg/m<sup>3</sup>. At M3 transition to the high season results in less dense water, whereas at M2 it’s the other way around, and at the moment we have no current explanation for this pattern.

[46] In terms of water dynamics, the M3 mooring exhibits a velocity signature that is distinctly different from that of the M2 mooring and the upstream data. The upstream observations across the West Spitsbergen Current by *Fahrbach et al.*

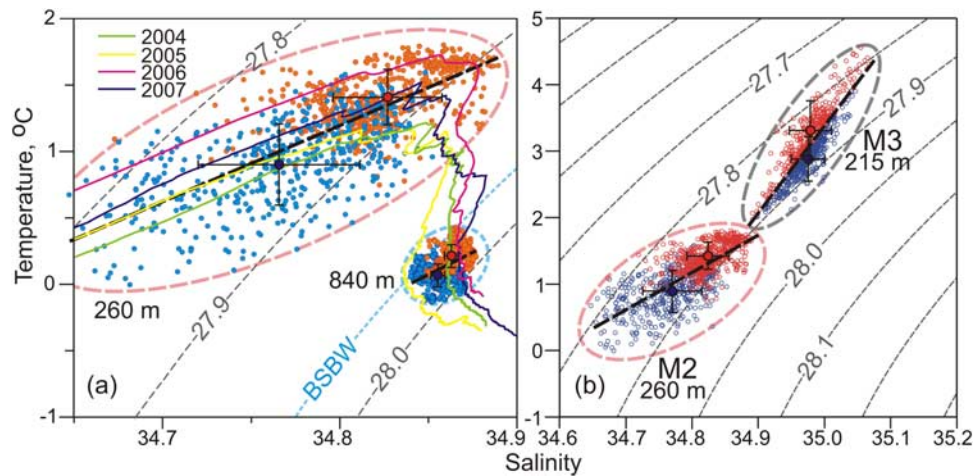


**Figure 11.** (a) The T-S scatterplot of the daily mean temperature and salinity time series (2004–2007) from the FSBW core ( $\sim 260$  m, contoured by pink dashed line) and the BSBW core ( $\sim 840$  m, contoured by blue dashed line) at the M2 mooring. Green, yellow, violet, and blue lines show CTD casts taken at the M2 mooring in September 2004, 2005, 2006, and 2007, respectively. The blue dashed line identifies the mean potential density of the BSBW following *Dmitrenko et al.* [2008b]. (b) The T-S scatterplot for the daily mean temperature and salinity time series (2004–2006) from the FSBW core at the M2 mooring ( $\sim 260$  m, contoured by pink dashed line) and the M3 mooring ( $\sim 215$  m, contoured by gray dashed line, adjusted from *Ivanov et al.* [2009]). (both) Red and blue dots depict T-S characteristics for “high” and “low” seasons, respectively. Red and blue error-barred dots show seasonal mean  $\pm 1$  standard deviation for “high” and “low” seasons, respectively. The linear regression is shown by bold dashed black lines. Dashed gray lines are sigma-0 isopycnals in  $\text{kg/m}^3$ .

[2001] revealed an AW flow seasonality with maximum FSBW transport in winter (February), and minimum transport in summer (August). At M2, downstream, the seasonal velocity signal is weak, but the record is dominated by high-frequency (likely mesoscale) velocity variability. In contrast to upstream and downstream, the 1-year-long velocity time series at M3 demonstrated neither a substantial seasonal signal in the FSBW along-slope boundary current nor high-frequency variability that could be attributed to the mesoscale eddies and/or meanders [*Ivanov et al.*, 2009]. It seems thus that the M2 seasonal pattern of high-frequency variability maybe introduced between M3 and M2, possibly by interactions between the FSBW and the BSBW, for examples instabilities on the front near St. Anna Trough as hypothesized by *Woodgate et al.* [2001] and all the others. This issue is discussed in the next subsection.

#### 5.4. BSBW Inflow

[47] The seasonality of the BSBW flow is commonly accepted [e.g., *Loeng et al.*, 1997] and well documented for both the BSO [*Furevik*, 2001; *Ingvaldsen et al.*, 2004a, 2004b] and the northeastern Barents Sea [*Loeng et al.*, 1993; *Loeng et al.*, 1997; *Schauer et al.*, 2002a]. This seasonality is closely connected to the seasonal variations in the regional atmospheric pressure fields. The southerly winds, which dominate during the winter, increase the wind-driven part of the AW inflow into the Arctic, while the weaker, more fluctuating easterly winds, which are common in the summer, decrease the wind-driven inflow [*Ingvaldsen et al.*, 2002]. In addition, local sea-ice and atmospheric forcing modify the background seasonal signal flowing into the Barents Sea through the BSO while the BSBW crosses the Barents Sea [*Martin and Cavalieri*,

1989; *Pfirman et al.*, 1994; *Schauer et al.*, 2002a; *Dmitrenko et al.*, 2009]. Here we examine the capacity of the BSBW inflow into the Arctic Ocean to modify the AW layer thermohaline and dynamic properties.

[48] To find the range of seasonal temperature and salinity amplitudes upstream over the Barents Sea the monthly mean values of temperature, salinity, and water depth for the sigma-0 isopycnals associated with the FSBW and the BSBW cores were computed over the northeastern Barents Sea using the data from the Climatic Atlas of the Arctic Seas 2004 [*Matishov et al.*, 2004]. The spatially distributed individual (snapshot) measurements taken in each particular month were linearly interpolated in a regular 100 km grid over the 200 km search radius. Then the depth, temperature, and salinity of sigma-0 isopycnals of  $27.860 \pm 0.040 \text{ kg/m}^3$  and  $27.985 \pm 0.015 \text{ kg/m}^3$  were calculated from the monthly mean vertical profiles for each grid node. An example of the long-term mean annual cycle constructed from the monthly data for the grid node at  $75^\circ\text{N}$  and  $50^\circ\text{E}$  is shown in Figure 12. The seasonal cycling is evident for both levels with maximum values in November and minimum values in April–May. The seasonal amplitudes of temperature and salinity for the “FSBW” and “BSBW” isopycnals at a position of  $75^\circ\text{N}$  and  $50^\circ\text{E}$  are  $1.3^\circ\text{C}$  and  $0.08 \text{ psu}$  and  $0.5^\circ\text{C}$  and  $0.02 \text{ psu}$ , respectively (Figure 12). These results are in agreement with yearlong mooring observations north of Novaya Zemlia by *Loeng et al.* [1993] [see also *Schauer et al.*, 2002a] showing temperature seasonal cycling down to at least 105 m with maximum values in October–November 1991 and minimum values in January–April 1992. In fact, seasonality is a feature characteristic of the entire northeastern Barents Sea as is illustrated by the significant seasonal difference between thermohaline char-

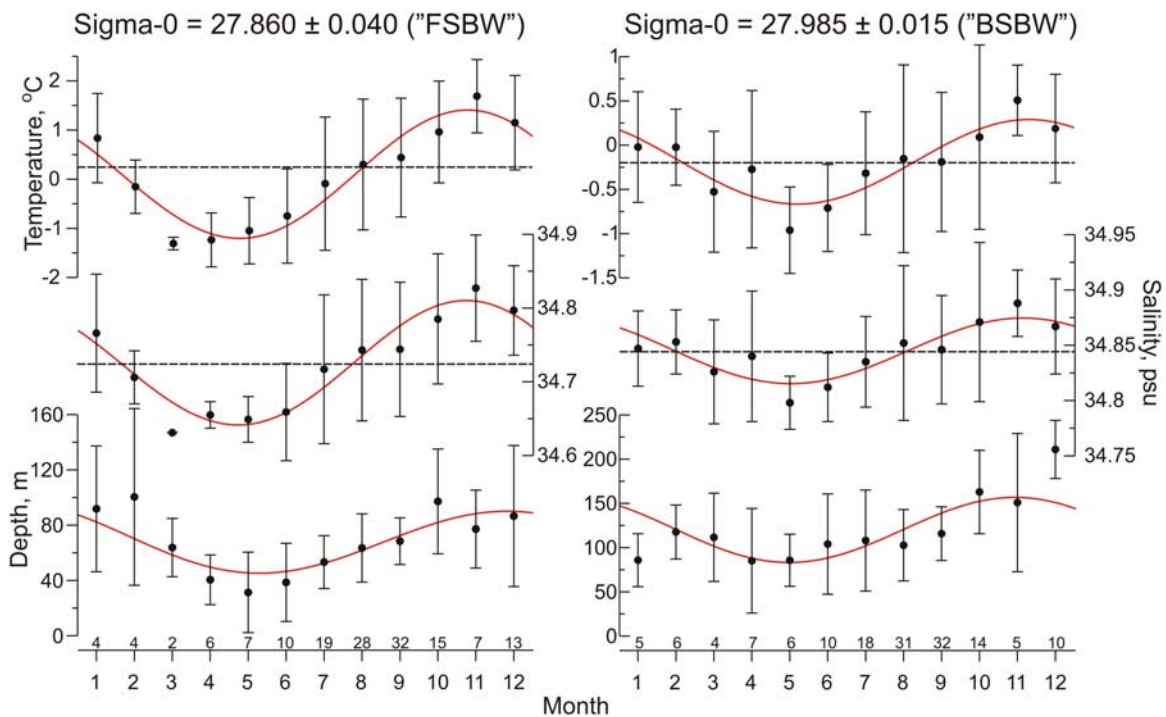


**Figure 12.** Monthly variability of temperature ( $^{\circ}\text{C}$ ), salinity (psu), and water depth (m) for a sigma-0 isopycnals of (left)  $27.860 \pm 0.040 \text{ kg/m}^3$  and (right)  $27.985 \pm 0.015 \text{ kg/m}^3$  over the eastern Barents Sea, corresponding to the approximate density of the cores of the FSBW and BSBW, respectively. Dots depict monthly means obtained by averaging over the area within a 200-km radius around  $75^{\circ}\text{N}$  and  $50^{\circ}\text{E}$ , a region of  $\sim 200\text{-m}$  water depth shown in Figure 13 by an open circle. Error bars depict  $\pm 1$  standard deviation. Red line shows a two-degree polynomial approximation. Number of years represented by hydrographical observations and employed for monthly mean estimation is at the top of bottom axis. Data are from the Climatic Atlas of the Arctic Seas 2004 [Matishov *et al.*, 2004].

acteristics calculated over the “FSBW” and “BSBW” isopycnals for a “high” season (November) and a “low” season (May), shown in Figure 13. Given the fact that the 840 m depth at M2 is dominated by the BSBW, we believe that the seasonality observed in thermohaline properties at this depth is caused by advection of the seasonal signal from the Barents Sea as follows from Figures 12 and 13.

[49] The analysis of the FSBW T-S properties at M2 reveals the possible role of upstream interaction between the FSBW and the BSBW in the seasonal modification of the FSBW at 260 m. Schauer *et al.* [2002b] suggested that the upper 500 m of the AW boundary current over the Amundsen Basin is conditioned by equal contributions from both AW branches, while at depths greater than 500 m the BSBW contribution is larger. Woodgate *et al.* [2001] inferred that the far-field effects of BSBW inflow over the shelf junction with the Lomonosov Ridge showed the capacity of the BSBW to modify the FSBW upper layer. Following this hypothesis, we argue that some part of the FSBW seasonal variability in the eastern Laptev Sea may be explained through its upstream interaction with the BSBW. The linear regression through the “low” and “high” season FSBW temperatures and salinities in the T-S scatterplot in Figure 11 (left) demonstrates an inclination similar to that of CTD profiles taken in September 2003–2007 at the M2 mooring. Furthermore, this regression line is consistent with the CTD cast taken in September 2005 through the upper

AW layer. In fact, during the “low” season the FSBW thermohaline properties are modified toward the overlying water properties (Figure 11, left) which are more strongly impacted by the fraction of the BSBW inflow that overlies the FSBW layer. Therefore seasonality observed at 260 m may be partially linked to the seasonal mixing of warmer and saltier FSBW with cooler and fresher BSBW. So the FSBW cooling and freshening we observe during the “low” season is partially due to a change in properties (or volume) of the end-members of this mixing process. For example, the FSBW could cool and freshen seasonally, or a seasonal decrease could occur in the volume of the FSBW relative to that of the BSBW; the latter seems to be the case given the fact of increased BSBW transport during the initial phase of the “low” season [Schauer *et al.*, 2002a]. Over the M2 region the cooler and fresher FSBW anomaly of January–April 1996 has been similarly explained by Woodgate *et al.* [2001], although it is curious that the change other their 1995–1996 mooring record was more isopycnal than those observed at M2. In contrast to the FSBW, the BSBW layer T-S regression exhibits no patterns that can be obviously linked to seasonal mixing with overlying FSBW (Figure 11, left).

[50] The additional evidence of interactions between the FSBW and the BSBW comes from comparing the upstream (M3) and the downstream (M2) FSBW salinity in Figure 11 (right). While the lateral and vertical salt fluxes may reduce

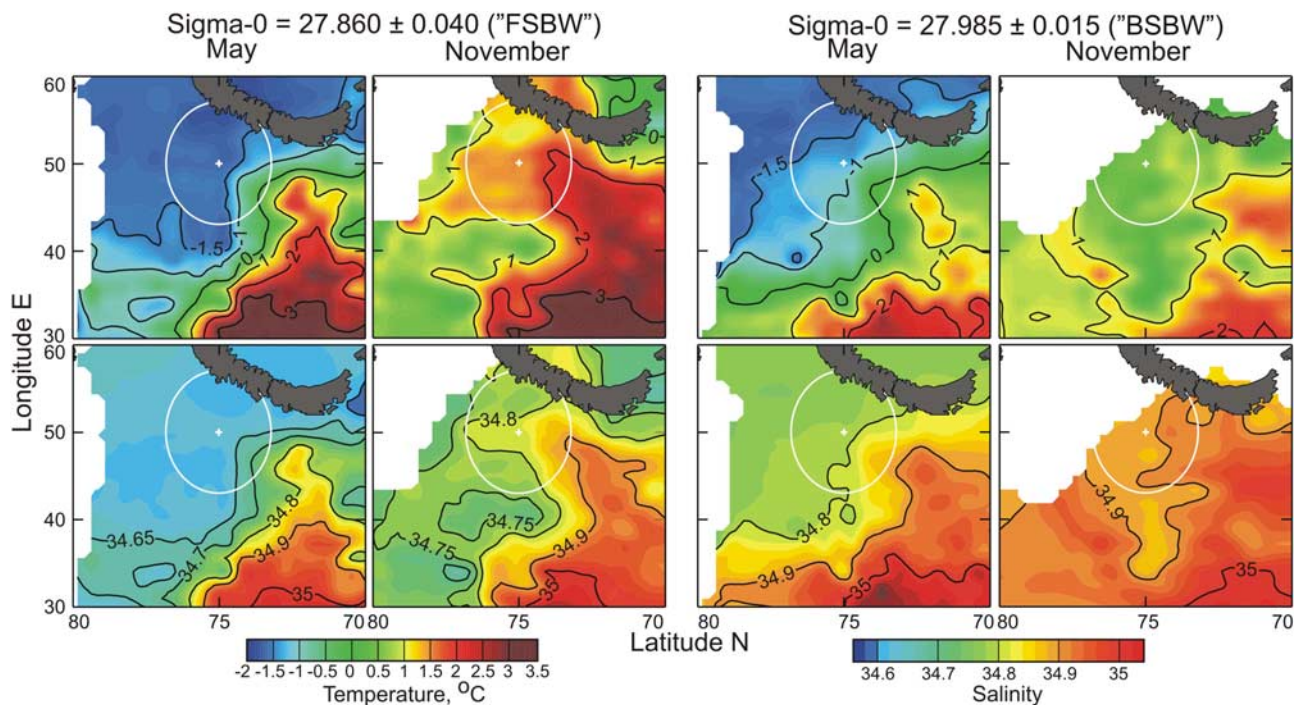


**Figure 13.** The gridded monthly mean (top) temperature ( $^{\circ}\text{C}$ ) and (bottom) salinity (psu) for May and November for sigma-0 isopycnals of (left)  $27.860 \pm 0.040 \text{ kg/m}^3$  and (right)  $27.985 \pm 0.015 \text{ kg/m}^3$ , corresponding to the approximate density of the cores of the FSBW and BSBW, respectively. Open circle with a center at  $75^{\circ}\text{N}$  and  $50^{\circ}\text{E}$  delineates the area of monthly mean calculations shown in Figure 12. Data are from the Climatic Atlas of the Arctic Seas 2004 [Matishov *et al.*, 2004]. Note that geographical orientation follows that of Figure 1. Blanked areas mark areas of insufficient data coverage.

the FSBW salinity as the FSBW translates downstream from Fram Strait, it is very likely that some portion of the FSBW freshening from  $\sim 34.97$  psu at the M3 mooring down to  $34.77$  psu at the M2 mooring (Figure 11, right) is due to interaction with relatively fresher BSBW over the northern Kara Sea.

[51] The seasonality in the Barents Sea outflow detected by Loeng *et al.* [1993] seems to be very important in terms of explaining the seasonal patterns of water dynamics observed at M2. We speculate that the occurrence of eddy-like features is linked to the seasonal variability in the intensity of the background AW flow. The upstream observations by Ivanov *et al.* [2009] at M3 north of Svalbard have revealed no substantial seasonality in the background FSBW flow. In contrast, Loeng *et al.* [1993] reported a seasonal increase in the intensity of the BSBW flow over the northeastern Barents Sea during winter months [see also Schauer *et al.*, 2002a]. Our projection of this result downstream to the confluence between the FSBW and the BSBW underlies our speculation that eddy-like features impact the seasonal signal while propagating from upstream to the M2 mooring.

[52] A maximum outflow from the northeastern Barents Sea to the northern Kara Sea was observed in December during a transitional period from a “high” to a “low” thermohaline season, which lagged the thermohaline cycle by about several months. The minimum outflow in August was revealed to be five times weaker than in December [Loeng *et al.*, 1993; Schauer *et al.*, 2002a]. Outflow of the BSBW to the Eurasian Basin occurs along the eastern flank

of the St. Anna Trough [Schauer *et al.*, 2002a]. If the BSBW maintains its identity through the northern Kara Sea, the seasonal signal in the BSBW transport would imply the susceptibility of a front, forming between the FSBW and the BSBW in or near the St. Anna Trough, to seasonal instability. Schauer *et al.* [1997] showed that downstream of the confluence between the FSBW and the BSBW, the AW boundary current can be baroclinically unstable. Near the formation region the front between the FSBW and the BSBW is sharpest and most unstable, but downstream, horizontal mixing between the FSBW and the BSBW erodes the front, leaving no clear horizontal distinction between the two branches [Woodgate *et al.*, 2001]. Furthermore, Woodgate *et al.* [2001] argued that inflow of the BSBW may exert an additional destabilizing effect on the FSBW. Schauer *et al.* [2002b] reported several deeper water lenses that were colder and lower in salinity than the ambient water, presumably formed from a cross-frontal interaction between the BSBW and the water beneath the FSBW core. They also demonstrated that the density distribution at several off-slope stations north of Severnaya Zemlya is consistent with a subsurface anticyclonic baroclinic eddy field. Dmitrenko *et al.* [2008b] reported an anticyclonic baroclinic eddy that maintained the identities of the FSBW and BSBW sources along the  $\sim 1000$  km pathway to the M1 mooring. Woodgate *et al.* [2001] suggested that eddies extending to depths of more than  $1000$  m near the junction of the Lomonosov Ridge with the Eurasian continental margin close to the M2 mooring (Figure 1) originate from an instability in the front that

forms between the FSBW and the BSBW. Finally, the M2 record provides evidence for seasonality in the occurrence of the mesoscale eddy-like features that are observed throughout the entire AW layer down to a depth of 840 m (Figures 3, 4, and 7–9). The occurrence of these mesoscale features is also associated with a seasonal increase in the intensity of the background AW boundary flow by  $\sim 2$ – $3$  times as is evident from our record (Figures 3, 4, and 7–9).

[53] All these facts allow the eddy-like features to be considered as a tracer released to the downstream propagating seasonal signal due to the instability of the front between the FSBW and the BSBW in the northern Kara Sea. The displacement between seasonality in water dynamics and thermohaline properties observed at the M2 mooring is generally consistent with that reported for the northeastern Barents Sea by Loeng *et al.* [1993]. The occurrence of the eddy-like features in the FSBW layer provides indirect evidence that the BSBW outflow from the Barents Sea is capable of modifying the FSBW thermohaline properties.

## 6. Conclusions and Final Remarks

[54] Our 3-year (2004–2007) mooring observational data collected in the eastern Eurasian basin at the eastern Laptev Sea continental slope suggest the existence of a seasonal signal, with generally higher temperature and salinity values from December–January to May–July and lower values from May–July to December–January. Our data show that the entire AW layer down to at least 840 m is affected by seasonal cycling, but the strength of the seasonal signal in temperature and salinity is substantially reduced from  $\pm 0.25^\circ\text{C}$  and  $\pm 0.025$  psu at 260 m to  $\pm 0.05^\circ\text{C}$  and  $\pm 0.005$  psu at 840 m. The magnitude of this seasonal signal rises above the level of noise attributed to shifting of the AW jet across the Siberian margin. The velocity seasonal signal is substantially weaker than that of the thermohaline cycle, is strongly hidden by high-frequency variability, and lags the thermohaline cycle by 45–75 day.

[55] We argue that our mooring record shows a time history of the AW seasonal signal which propagates along-margin and is carried from upstream by the AW boundary current. We eliminate ventilation through the coastal polynyas as a possible source of seasonality since polynya water has little ability to affect the entire AW layer on a regular seasonal basis, as required by our data. Our analysis suggests that the seasonal signal in the FSBW warm core (at 260 m) is predominantly translated from Fram Strait, while the seasonality in the BSBW domain (at 840 m) is instead attributable to the seasonal signal inherited from the Barents Sea. At the same time, the characteristic signature of the BSBW seasonal dynamics observed throughout the entire AW layer leads us to speculate that the BSBW has a role in modifying the seasonal properties of the FSBW. The signature of interaction between the FSBW and the BSBW over the mouth of St. Anna Trough in the northern Kara Sea is traced downstream in the northeastern Laptev Sea through mesoscale eddy-like activity that affects the entire AW layer. We consider the quasi-seasonal occurrence of these eddy-like patterns to be a tracer of seasonal variability of the AW layer dynamics downstream of the FSBW/BSBW confluence zone. In this context, it is very likely that the BSBW contribution to

the heat and salt balance of the Arctic Ocean intermediate waters is currently underestimated.

[56] Although our data are not sufficient to allow us to draw final conclusions, it is evident that the seasonal signal strongly modifies the AW properties even thousands of kilometers away from the source of the AW inflow. While some of our discussion and conclusions are necessarily speculative, the data show an intriguing seasonal signal embedded in the two branches of the Atlantic inflow into the Arctic Ocean, indicating the complexity of the subsurface physical oceanography and heat and salt transport. Further upstream investigations are needed to test our hypothesis. This research should be based on modeling of the area and on improved in situ measurements, especially in the area of the confluence of the two branches in the mouth of the St. Anna Trough.

[57] Finally, and importantly, our results are cautionary for the interpretation of “snapshots” of spatially distributed oceanographic data. An along-margin propagating seasonal signal with an amplitude of  $0.5$ – $1.0^\circ\text{C}$  produces “spatial” noise that should be taken into account when analyzing the snapshot CTD information: annual sampling may well be aliasing the changing AW temperature, with implications for how we have interpreted CTD data in the past. In addition, any large-scale thermodynamic warming must rise above the level of seasonal “noise” to be properly detected by a single 1-yearlong mooring record.

[58] **Acknowledgments.** The hydrographic observations in 2003–2007 were carried out within the working framework of the ongoing NOAA and NSF-funded IARC Program “Nansen and Amundsen Basins Observational System” (NABOS). The M2 mooring is maintained, thanks to funding through the Network of Centres of Excellence of Canada: ArcticNet. I.D. and S.K. gratefully acknowledge the financial support through the BMBF project “System Laptev Sea” (03G0639A). I.P. and V.I. thank the Frontier Research System for Global Change for financial support. R.W. acknowledges support from NSF grant ARC-0454843. N.K. was supported by a grant from the IMPRS-ESM (International Max Planck Research School on Earth System Modeling). D.B. appreciates funds through the DFG grant SP 526/3 and the BMBF project “System Laptev Sea” (03G0639D). We greatly appreciate Ursula Schauer for her helpful comments and discussions.

## References

- Aagaard, K. (1989), A synthesis of the Arctic Ocean circulation, *Rapp. P. V. Reun. Cons. Int. Explor. Mer.*, *188*, 11–22.
- Bareiss, J., and K. Gørgen (2005), Spatial and temporal variability of sea ice in the Laptev Sea: Analyses and review of satellite passive-microwave data and model results, 1979 to 2002, *Global Planet. Change*, *48*(1–3), 28–54, doi:10.1016/j.gloplacha.2004.12.004.
- Carmack, E., K. Aagaard, J. Swift, R. Perkin, F. McLaughlin, R. Macdonald, P. Jones, J. Smith, K. Ellis, and L. Kilius (1997), Changes in temperature and tracer distributions within the Arctic Ocean: Results from the 1994 Arctic Ocean Section, *Deep Sea Res. Part II*, *44*, 1487–1502, doi:10.1016/S0967-0645(97)00056-8.
- Chapman, D. C. (1999), Dense water formation beneath a time-dependent coastal polynya, *J. Phys. Oceanogr.*, *29*(4), 807–820.
- Chapman, D. C. (2000), The influence of an alongshelf current on the formation and offshore transport of dense water from a coastal polynya, *J. Geophys. Res.*, *105*(C10), 24,007–24,019.
- Dethleff, D., P. Loewe, and E. Kline (1998), Detailed investigation on ice formation and export during 1991/1992 winter season, *Cold Reg. Sci. Technol.*, *27*, 225–243.
- Dickson, R. R., T. J. Osborn, J. W. Hurrell, J. Meincke, J. Blindheim, B. Adlandsvik, T. Vinje, G. Alekseev, and W. Maslowski (2000), The Arctic Ocean response to the North Atlantic Oscillation, *J. Clim.*, *13*(15), 2671–2696.
- Dmitrenko, I. A., I. V. Polyakov, S. A. Kirillov, L. A. Timokhov, H. L. Simmons, V. V. Ivanov, and D. Walsh (2006), Seasonal variability of Atlantic water on the continental slope of the Laptev Sea during 2002–2004, *Earth Planet. Sci. Lett.*, *244*(3–4), 735–743, doi:10.1016/j.epsl.2006.01.067.

- Dmitrenko, I. A., et al. (2007), NABOS-06 expedition in the Eurasian Basin aboard the icebreaker Kapitán Dranitsyn (August–September 2006), *IARC Tech. Rep.*, 4, 9–80.
- Dmitrenko, I. A., I. V. Polyakov, S. A. Kirillov, L. A. Timokhov, I. E. Frolov, V. T. Sokolov, H. L. Simmons, V. V. Ivanov, and D. Walsh (2008a), Toward a warmer Arctic Ocean: Spreading of the early 21st century Atlantic Water warm anomaly along the Eurasian Basin margins, *J. Geophys. Res.*, 113, C05023, doi:10.1029/2007JC004158.
- Dmitrenko, I. A., S. A. Kirillov, V. V. Ivanov, and R. A. Woodgate (2008b), Mesoscale Atlantic water eddy off the Laptev Sea continental slope carries the signature of upstream interaction, *J. Geophys. Res.*, 113, C07005, doi:10.1029/2007JC004491.
- Dmitrenko, I. A., D. Bauch, S. A. Kirillov, N. Koldunov, P. J. Minnett, V. V. Ivanov, J. A. Hölemann, and L. A. Timokhov (2009), Barents Sea upstream events impact the properties of Atlantic water inflow into the Arctic Ocean: Evidence from 2005–2006 downstream observations, *Deep Sea Res., Part 1*, 56(4), 513–527, doi:10.1016/j.dsr.2008.11.005.
- Fahrbach, E., J. Meincke, S. Osterhus, G. Rohardt, U. Schauer, V. Tverberg, and J. Verduin (2001), Direct measurements of volume transports through Fram Strait, *Polar Res.*, 20(2), 217–224.
- Falkner, K., M. Steele, R. Woodgate, J. Swift, K. Aagaard, and J. Morison (2005), Dissolved oxygen extrema in the Arctic Ocean halocline from the North Pole to the Lincoln Sea, *Deep Sea Res., Part 1*, 52(7), 1138–1154.
- Foufoula-Georgiou, E., and P. Kumar (Eds.) (1995), *Wavelets in Geophysics*, 373 pp., Academic, San Diego, Calif.
- Furevik, T. (2001), Annual and interannual variability of Atlantic water temperatures in the Norwegian and Barents Seas: 1980–1996, *Deep Sea Res., Part 1*, 48, 383–404.
- Gawarkiewicz, G. (2000), Effects of ambient stratification and shelfbreak topography on offshore transport of dense water on continental shelves, *J. Geophys. Res.*, 105(C2), 3307–3324.
- Ingvaldsen, R., H. Loeng, and L. Asplin (2002), Variability in the Atlantic inflow to the Barents Sea based on a one-year time series from moored current meters, *Cont. Shelf Res.*, 22(3), 505–519.
- Ingvaldsen, R. B., L. Asplin, and H. Loeng (2004a), Velocity field of the western entrance to the Barents Sea, *J. Geophys. Res.*, 109, C03021, doi:10.1029/2003JC001811.
- Ingvaldsen, R. B., L. Asplin, and H. Loeng (2004b), The seasonal cycle in the Atlantic transport to the Barents Sea during the years 1997–2001, *Cont. Shelf Res.*, 24(9), 1015–1032.
- Ingvaldsen, R. B. (2005), Width of the North Cape Current and location of the Polar Front in the western Barents Sea, *Geophys. Res. Lett.*, 32, L16603, doi:10.1029/2005GL023440.
- Ivanov, V. V., and P. N. Golovin (2007), Observations and modeling of dense water cascading from the northwestern Laptev Sea shelf, *J. Geophys. Res.*, 112, C09003, doi:10.1029/2006JC003882.
- Ivanov, V. V., I. V. Polyakov, I. A. Dmitrenko, E. Hansen, I. A. Repina, S. A. Kirillov, C. Mauritzen, H. Simmons, and L. A. Timokhov (2009), Seasonal variability in Atlantic Water off Spitsbergen, *Deep Sea Res., Part 1*, 56(1), 1–14, doi:10.1016/j.dsr.2008.07.013.
- Jakobsson, M., and IBCAO Editorial Board Members (2001), Improvement to the International Bathymetric Chart of the Arctic Ocean (IBCAO): Updating the data base and the grid model, *Eos Trans. AGU*, 82(47), Fall Meet. Suppl., Abstract OS11B-0371.
- Karcher, M. J., R. Gerdes, F. Kauker, and C. Koberle (2003), Arctic warming: Evolution and spreading of the 1990s warm event in the Nordic seas and the Arctic Ocean, *J. Geophys. Res.*, 108(C2), 3034, doi:10.1029/2001JC001265.
- Killworth, P. D. (1992), An equivalent-barotropic mode in FRAM, *J. Phys. Oceanogr.*, 22(11), 1379–1387.
- Loeng, H., V. Ozhigin, B. Ardlandsvik, and H. Sagen (1993), Current measurements in the northeastern Barents Sea, in *Proceedings, ICES Statutory Meeting 1993, C. M. 1993/C:41*, 22 pp., Int. Council for the Explor. of the Sea, Copenhagen.
- Loeng, H., V. Ozhigin, and B. Ardlandsvik (1997), Water fluxes through the Barents Sea, *ICES, J. Mar. Sci.*, 54, 310–317.
- Martin, S., and D. J. Cavalieri (1989), Contributions of the Siberian Shelf polynyas to the Arctic Ocean intermediate and deep water, *J. Geophys. Res.*, 94(C9), 12,725–12,738.
- Matishov, G., et al. (2004), Climatic Atlas of the Arctic Seas 2004, in *NOAA Atlas NESDIS 58, World Data Center for Oceanography—Silver Spring, Int. Ocean Atlas and Information Ser.*, vol. 9, 148 pp., U.S. Government Printing Office, Washington, D. C. [CD-ROM].
- McLaughlin, F. A., E. C. Carmack, R. W. Macdonald, A. Weaver, and J. N. Smith (2002), The Canada Basin 1989–1995: Upstream events and far-field effects of the Barents Sea, *J. Geophys. Res.*, 107(C7), 3082, doi:10.1029/2001JC000904.
- Morison, J. (1991), Seasonal variations in the West Spitsbergen Current estimated from bottom pressure measurements, *J. Geophys. Res.*, 96(C10), 18,381–18,395.
- Pfirman, S. L., D. Bauch, and T. Gammelsrød (1994), The Northern Barents Sea: Water mass distribution and modification, in *The Polar Oceans and Their Role in Shaping the Global Environment: The Nansen Centennial Volume, Geophys. Monogr. Ser.*, vol. 85, edited by O. M. Johannessen, R. D. Muench, and J. E. Overland, pp. 77–94, AGU, Washington, D. C.
- Polyakov, I., et al. (2005), One more step toward a warmer Arctic, *Geophys. Res. Lett.*, 32, L17605, doi:10.1029/2005GL023740.
- Polyakov, I., et al. (2007), Observational program tracks Arctic Ocean transition to a warmer state, *Eos Trans. AGU*, 88(40), 398, doi:10.1029/2007EO400002.
- Quadfasel, D., A. Sy, D. Welles, and A. Tunik (1991), Warming in the Arctic, *Nature*, 350, 385.
- Rudels, B., E. P. Jones, L. G. Anderson, and G. Kattner (1994), On the intermediate depth waters of the Arctic Ocean, in *The Polar Oceans and Their Role in Shaping the Global Environment: The Nansen Centennial Volume, Geophys. Monogr. Ser.*, vol. 85, edited by O. M. Johannessen, R. D. Muench, and J. E. Overland, pp. 33–46, AGU, Washington, D. C.
- Schauer, U., R. D. Muench, B. Rudels, and L. Timokhov (1997), Impact of eastern Arctic shelf waters on the Nansen Basin intermediate layers, *J. Geophys. Res.*, 102(C2), 3371–3382.
- Schauer, U., H. Loeng, B. Rudels, V. K. Ozhigin, and W. Dieck (2002a), Atlantic Water flow through the Barents and Kara Seas, *Deep Sea Res. I*, 49(12), 2281–2298, doi:10.1016/S0967-0637(02)00125-5.
- Schauer, U., B. Rudels, E. P. Jones, L. G. Anderson, R. D. Muench, G. Björk, J. H. Swift, V. Ivanov, and A. M. Larsson (2002b), Confluence and redistribution of Atlantic water in the Nansen, Amundsen and Makarov basins, *Ann. Geophys.*, 20(2), 257–273.
- Schauer, U., E. Fahrbach, S. Osterhus, and G. Rohardt (2004), Arctic warming through the Fram Strait: Oceanic heat transport from three years of measurements, *J. Geophys. Res.*, 109(C6), C06026, doi:10.1029/2003JC001823.
- Smolyar, I., and N. Adrov (2003), The quantitative definition of the Barents Sea Atlantic Water: Mapping of the annual climatic cycle and interannual variability, *ICES J. Mar. Sci.*, 60(4), 836–845.
- Spreen, G., and L. Kaleschke (2008), *AMSR-E ASI 6.25 km Sea Ice Concentration Data, V5.4*, Inst. of Oceanography, Univ. of Hamburg, Germany, digital media (ftp-projects.zmaw.de/seaice/).
- Spreen, G., L. Kaleschke, and G. Heygste (2008), Sea ice remote sensing using AMSR-E 89 GHz channels, *J. Geophys. Res.*, 113, C02S03, doi:10.1029/2005JC003384.
- Timofeev, V. T. (1957), Atlantic waters in the Arctic basin (in Russian), *Probl. Arkt. Antarkt.*, 2, 41–52.
- Walsh, D., I. Polyakov, L. Timokhov, and E. Carmack (2007), Thermohaline structure and variability in the eastern Nansen Basin as seen from historical data, *J. Mar. Res.*, 65(5), 685–714, doi:10.1357/002224007783649466.
- Woodgate, R. A., K. Aagaard, R. D. Muench, J. Gunn, G. Björk, B. Rudels, A. T. Roach, and U. Schauer (2001), The Arctic Ocean boundary current along the Eurasian slope and the adjacent Lomonosov Ridge: Water mass properties, transports and transformations from moored instruments, *Deep Sea Res. Part 1*, 48, 1757–1792.
- Woodgate, R. A., K. Aagaard, J. H. Swift, W. M. Smethie Jr., and K. K. Falkner (2007), Atlantic water circulation over the Mendeleev Ridge and Chukchi Borderland from thermohaline intrusions and water mass properties, *J. Geophys. Res.*, 112, C02005, doi:10.1029/2005JC003416.

D. Bauch and I. A. Dmitrenko, Department of Paleoceanography, Leibniz Institute of Marine Sciences, University of Kiel, Wischhofstrasse 1-3, D-24148 Kiel, Germany. (idmitrenko@ifm-geomar.de)

L. Fortier and C. Lalonde, Laval University, Pavillon Alexandre-Vachon, 1045, av. de la Médecine, Québec City, QC G1V 0A6, Canada.

J. A. Hölemann, Alfred Wegener Institute for Polar and Marine Research, Am Handelshafen 12, D-27570 Bremerhaven, Germany.

V. V. Ivanov, Dunstaffnage Marine Laboratory, Scottish Association for Marine Science, Oban PA34 4AD, UK.

L. Kaleschke, Institute of Marine Sciences, University of Hamburg, Bundesstr. 53, 20146 Hamburg, Germany.

S. A. Kirillov and L. A. Timokhov, Department of Oceanology, Arctic and Antarctic Research Institute, 38 Bering Str., 199397 St. Petersburg, Russia.

N. Koldunov, International Max Planck Research School on Earth System Modelling, Bundesstr. 53, D-20146 Hamburg, Germany.

I. V. Polyakov, International Arctic Research Center, University of Alaska, P.O. Box 757340, 930 Koyukuk Drive, Fairbanks, AK 99775-7340, USA.

R. A. Woodgate, Polar Science Center, Applied Physics Laboratory, University of Washington, P.O. Box 355640, 1013 NE 40th Street, Seattle, WA 98105-6698, USA.